

# Hulk: A Universal Knowledge Translator for Human-Centric Tasks

Yizhou Wang\*, Yixuan Wu\*, Shixiang Tang✉, Weizhen He, Xun Guo, Feng Zhu, Lei Bai, Rui Zhao, Jian Wu, *Member, IEEE*, Tong He, Wanli Ouyang, *Senior Member, IEEE*

arXiv:2312.01697v2 [cs.CV] 5 Dec 2023

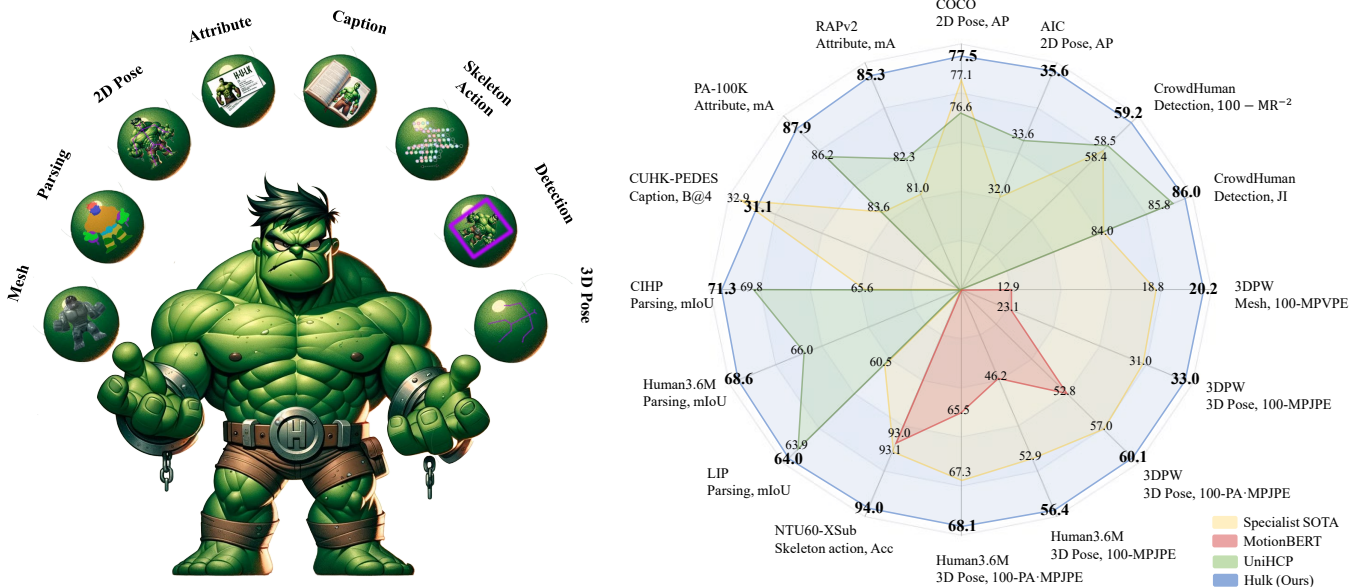


Fig. 1: **Left:** Our proposed Hulk is a general human-centric perceiver that can tackle major 2D vision, 3D vision, skeleton-based, and vision language tasks using a unified framework. **Right:** Hulk pushes the limits on various human-centric tasks when compared with specialist models, pretraining models, *e.g.*, MotionBERT [1], and existing generalist models, *e.g.*, UniHCP [2].

**Abstract**—Human-centric perception tasks, *e.g.*, human mesh recovery, pedestrian detection, skeleton-based action recognition, and pose estimation, have wide industrial applications, such as metaverse and sports analysis. There is a recent surge to develop human-centric foundation models that can benefit a broad range of human-centric perception tasks. While many human-centric foundation models have achieved success, most of them only excel in 2D vision tasks or require extensive fine-tuning for practical deployment in real-world scenarios. These limitations severely restrict their usability across various downstream tasks and situations. To tackle these problems, we present Hulk, the first multimodal human-centric generalist model, capable of addressing most of the mainstream tasks simultaneously without task-specific finetuning, covering 2D vision, 3D vision, skeleton-based, and vision-language tasks. The key to achieving this is condensing various task-specific heads into two general heads, one for discrete representations, *e.g.*, languages, and the other for continuous representations, *e.g.*, location coordinates. The outputs of two heads can be further stacked into four distinct input and output modalities. This uniform representation enables Hulk to treat human-centric tasks as modality translation, integrating knowledge across a wide range of tasks. To validate the effectiveness of our proposed method, we conduct comprehensive experiments on 11 benchmarks across 8 human-centric tasks. Experimental results surpass previous methods substantially, demonstrating the superiority of our proposed method. The code will be available on <https://github.com/OpenGVLab/HumanBench>.

**Index Terms**—Computer Vision, Human-centric Perception, Foundation Models, Multimodal Learning, Multitask Learning.

## I. INTRODUCTION

RECENT years have witnessed increasing research attention to human-centric tasks, *e.g.*, person re-identification [3]–[6], pose estimation [7]–[10], and human mesh recovery [1], [11], due to their widespread applications, including sports analysis [12]–[14], surveillance [15]–[18], augmented reality [19]–[21], and video production [22]–[24].

Most of the previous methods have typically emphasized unique designs tailored for individual tasks, involving heavy work for task-specific design, fine-tuning, and deployment. This lack of flexibility and adaptability constrained their applications in real-world scenarios, where multiple tasks are related and need to be addressed using a single model. To this end, some works have explored learning general representative encoders, also known as human-centric foundation

\*Yizhou Wang and Yixuan Wu are contributed equally. ✉Shixiang Tang is the corresponding author. This work was done when Yixuan Wu, Xun Guo were interns at Shanghai AI Laboratory, Shanghai, China. Yixuan Wu is with the School of Medicine, Zhejiang University, Hangzhou, 310027, China. Weizhen He is with the College of Electrical Engineering, Zhejiang University, Hangzhou, 310027, China. Xun Guo is with the Department of Automation, University of Science and Technology of China, Hefei, 230052, China. Shixiang Tang is with the School of Electrical and Information Engineering, University of Sydney, NSW, Australia. Feng Zhu and Rui Zhao are with SenseTime Group Limited, China. Jian Wu is with School of Public Health, Zhejiang University, Hangzhou, 310058, China. Yizhou Wang, Lei Bai, Tong He, and Wanli Ouyang are with Shanghai AI Laboratory, Shanghai, 200232, China.

models, that can be fine-tuned or prompt-tuned for different human-centric visual tasks. These models leverage large-scale pretraining on diverse datasets and have achieved remarkable performance across a wide range of tasks, particularly in 2D vision applications such as person re-identification [3]–[6], pose estimation [7]–[9], and human parsing [25]–[27]. Some notable examples of such models include SOLIDER [28], HCMoCo [62], MotionBERT [1], PATH [29], HAP [30], and SMPLer-X [31].

Despite the success of human-centric foundation models, these models still need to be tuned, making them fall short of the ultimate goal of the *general human-centric perceiver* - one versatile model for all tasks. This goal is inspired by developments in Natural Language Processing (NLP), where one model and one set of parameters, *e.g.*, ChatGPT [32] and InternLM [33], can address all NLP tasks. However, it remains challenging for human-centric tasks because of the diverse data formats and task modeling:

- Heterogeneous and multimodal inputs and outputs. Human-centric perception tasks typically include 2D vision tasks, 3D vision tasks, skeleton-based tasks, and vision-language tasks, whose inputs and outputs cover diverse formats, *i.e.*, images, languages, key points, segmentation maps, and categories. Unifying these incredibly heterogeneous inputs and outputs is nontrivial for a general human-centric perceiver.
- Highly specialized state-of-the-art model designs for individual human-centric tasks. Current state-of-the-art methods for human-centric tasks differ in backbones (*e.g.*, GNN [34] for skeleton-based action recognition and HRFFormer [35] for pose estimation) and task heads (*e.g.*, class guidance blocks [104] for human parsing and progressive dimensionality reduction heads [138], [143] for mesh recovery). Unifying these specialized but effective architectural designs for unique tasks is demanding for developing the general human-centric perceiver.

The most recent effort to approximate the abilities of the average human perceiver is represented by UniHCP [2]. This method employs a unified decoder coupled with a versatile yet target-driven interpreter, enabling it to tackle five 2D human-oriented visual challenges. However, the method struggles when dealing with several crucial human-centric tasks, including 3D vision tasks, vision-language tasks, and skeleton-based motion tasks (*e.g.*, skeleton-based action recognition) due to its encoder being only feasible for images. Besides, it fails to enhance the collaboration between various tasks. Consequently, the performance of certain tasks remains significantly lower than the cutting-edge specialized methods.

In this paper, we present Hulk, a Human-centric universal knowledge translator, as a *general human-centric perceiver*. Hulk is capable of handling major large-scale 2D vision, 3D vision, skeleton-based, and vision-language tasks listed in Table I. Compared to previous methods, its success results from the unification of both diverse input and output formats, and specialized architecture designs. First, Hulk condenses diverse task inputs and outputs into only two basic formats, *e.g.*, continuous digits and discrete words, which can be

further stacked into four modalities, *i.e.*, *Text* - discrete natural language tokens; *Image* - normalized RGB images with continuous values from 0 to 1; *Sparse Label* - 2D/3D continuous location coordinates plus discrete words as its semantic meanings; *Dense Label* - per-pixel discrete natural language tokens such as segmentation maps. Compared with existing human-centric models, we avoid designing heterogeneous task heads but explore the use of four modality tokenizers/de-tokenizers. These more concise formats facilitate better flexibility and scalability to various tasks and datasets. Second, Hulk reformulates diverse human-centric multimodal tasks into the modality translation task and accordingly unifies different task-specialist model designs into the encoder-decoder architecture similar to models in the machine translation task. The intuition behind is that if the *general human-centric perceiver* clearly perceives 2D and 3D information of human beings in an image, skeletons, or pedestrian appearance descriptions, we only need to teach it to translate between any input and output modalities. Inspired by advances in machine translation [38], [39], Hulk unifies different task-specialist designs into three simple and effective components: a modality-shared encoder and decoder, a modality-specialised data tokenizers before the encoder and token de-tokenizers after the decoder, and a modality-specialist indicator before the decoder to tell the decoder which modality the inputs should be translated to. Hulk first transforms multimodal data into token sequences in a common manifold space. The modality-shared encoder then extracts general human-centric representations from the token sequence. The modality-specialist indicator guides the modality-shared decoder to translate the human-centric representations into the tokens of the output modality. Finally, the modality-specialist de-tokenizer reconstructs the tokens into the desired output modalities.

To the best of our knowledge, Hulk is the first *generalist human-centric perceiver* achieving competitive results on major large-scale 2D vision, 3D vision, skeleton-based and vision-language multimodal human-centric tasks<sup>1</sup>, including pedestrian attribute recognition, pedestrian detection, 2D pose estimation, human parsing, pedestrian image caption, skeleton-based action recognition, 3D pose estimation and 3D human mesh recovery. Trained on a massive collection of about 30 million labeled human-centric datasets of eight tasks, Hulk can directly handle a broad range of tasks without further task-specific adaptation, even pushing the performance limits of the existing state-of-the-art methods. Specifically, as shown in Fig. 1, Hulk outperforms current leading human-centric specialist models and pretraining models by **+1.5%** mIoU on CIHP for human paring, **+3.1%** mA on RAPv2 for pedestrian attribute recognition, **+2.0%** AP on AIC for 2D pose estimation, **-0.7%**  $MR^{-2}$  (Missing rate) on CrowdHuman for pedestrian detection, **-1.4** MPVPE (Mean-Per-Vertex-Position-Error) and **-2.0** MPJPE (Mean-Per-Joint-Position-Error) on 3DPW for mesh recovery and 3D pose estimation, respectively.

To summarize, our contributions are three folds:

- We propose Hulk, the first *general human-centric per-*

<sup>1</sup>Tasks such as person re-identification and person search are not explored due to human ethical considerations.

TABLE I

SUPPORTING TASKS OF EXISTING HUMAN-CENTRIC PRETRAINING MODELS AND GENERALIST MODELS. PRETRAINING MODELS REQUIRE FINE-TUNING FOR DOWNSTREAM TASKS, WHEREAS GENERALIST MODELS LIKE HULK CAN BE DIRECTLY USED. COMPARED WITH OTHER METHODS, HULK CAN PERFORM ALL MENTIONED TASKS USING SHARED PARAMETERS EXCEPT FOR PERSON REID AND PERSON SEARCH DUE TO ETHICAL CONCERNs.

Task Type	Tasks	Pretraining					Generalist	
		HCMoCo	SOLIDER	PATH	HAP	MotionBERT	UniHCP	Hulk (ours)
2D Vision Tasks	Person ReID		✓	✓	✓		✓	
	Person Search		✓					
	Human Parsing	✓	✓	✓			✓	✓
	2D Pose Estimation	✓	✓	✓	✓		✓	✓
	Pedestrian Detection	✓	✓	✓			✓	✓
	Attribute Recognition	✓	✓	✓			✓	✓
Skeleton-based Tasks	Skeleton-based action				✓	✓		✓
Vision-language Tasks	Image Caption							✓
3D Vision Tasks	Mesh Recovery				✓	✓		✓
	3D Pose Estimation	✓			✓	✓		✓

ceiver capable of handling 2D vision tasks, 3D vision tasks, skeleton-based tasks, and vision-language tasks without task-specific fine-tuning.

- To facilitate unified modeling, we propose to design only two types of basic blocks, *i.e.*, one for predicting semantics and the other for predicting locations, to establish tokenizers and de-tokenizers of the output modalities.
- Hulk pushes the performance limits of 8 human-centric tasks, including 2D vision tasks, 3D vision tasks, skeleton-based tasks, and vision-language tasks.

## II. RELATED WORK

### A. Multimodal Foundation Models

Multimodal foundation models have emerged as a significant research direction towards artificial general intelligence (AGI), which aims to synthesize information from various sensory inputs to create more comprehensive AI systems.

Alignment with paired multimodal data, as one common way to develop multimodal foundation models, can be generally divided into two different categories: (1) **Contrastive methods**, which utilize contrastive loss to pull features with the same content close and push features with different contents apart. A famous example is CLIP [40], which aligns image-text pairs on websites, achieving remarkable zero-shot classification performance. VideoCLIP [41] and AudioCLIP [42] further extend this idea to alignments text with video and audio, respectively. ImageBind [43] binds five different modalities with images, achieving strong zero-/few-shot performance on cross-modality recognition tasks. (2) **Multimodel reconstruction methods**, which learn modality-agnostic representation through multi-modal masked autoencoding [44], [45]. For instance, MultiMAE [46] utilizes a modality-share encoder with modality-specific decoders to reconstruct masked RGB, depth and semantic patches, achieving desirable performance on downstream tasks in these modalities. MaskedVLM [47] and SMAUG [48] adopt masked image/text modeling to learn general representations for vision-language tasks. However, these methods focus on feature alignment and require additional task heads with fine-tuning for effective application in downstream perception tasks.

The recent emergence of multimodal large language models (MLLM) [49]–[58] proposes a new approach to handling diverse perception tasks: aligning all modalities into language and formatting all perception tasks into Visual Question Answering (VQA) tasks. Leveraging effective adaptation methods, *e.g.*, LoRA [59] and LLAMA-Adapter [60], MLLM generates language answers using the given samples in different modalities, including image [51]–[53], video [54], [55], point cloud [55]–[57], [61] and audio [55], [58]. Despite their versatility, MLLMs have not attained state-of-the-art performance in some perception tasks [49], [50], such as detection and mesh recovery. In this paper, we summarize the input/output of diverse human-centric tasks into four general modalities. Instead of aligning different modalities to a certain modality, we propose to treat all human-centric tasks as modality translation, thereby enhancing the model’s adaptability and scalability across diverse human-centric tasks using a versatile and effective framework.

### B. Human-Centric Foundation Models

Human-centric foundation models are pivotal in real-world applications, such as social surveillance, sports analysis, and *etc.* Depending on the model structures, they can be categorized into two types: (1) **Human-centric Pretraining Models** [28]–[30], [62], which introduce the human prior to pretrain a versatile backbone for extracting general human-centric representation. Specifically, HCMoCo [62] and HAP [30] leverage the offline extracted human keypoints as the prior knowledge to learn structure-invariant representation across diverse human poses, while SOLIDER [28] proposes to learn representation with more semantic information using token-level semantic classification pretext task. Despite the success, these models still require additional task-specific finetuning for downstream task applications due to their lack of unified task modeling. (2) **Human-centric General Perceivers** [2], aim for a unified framework to handle diverse human-centric tasks with task-specific finetuning. A notable example, UniHCP [2], introduces a shared decoder head with a task-guided interpreter to handle five 2D vision human-centric tasks without additional task-specific finetuning. Our proposed Hulk aligns with

TABLE II  
INPUT AND OUTPUT MODALITIES OF EIGHT COVERED HUMAN-CENTRIC TASKS. HULK TREATS ALL THESE TASKS AS MODALITY TRANSLATION. <sup>†</sup>IN THE MESH RECOVERY TASK, MANY VERTICES DO NOT HAVE A NAME THEREFORE WE ONLY PREDICT THEIR LOCATIONS.

Task	Input modality	Input sample	Output modality	Output sample
Human Parsing	Image	$\mathbf{x}_I$	Dense label	semantic map representing the occurrence of “hair”
2D Pose Estimation	Image	$\mathbf{x}_I$	Dense label	semantic map representing the occurrence of “nose”
Pedestrian Attribute Recognition	Image	$\mathbf{x}_I$	Text	“female”, “age 22-30”
Image Caption	Image	$\mathbf{x}_I$	Text	“A man with black suit standing near the bus station”
Pedestrian Detection	Image	$\mathbf{x}_I$	Sparse label	“pedestrian”, [0.12, 0.45, 0.21, 0.6]
3D Pose Estimation	Image	$\mathbf{x}_I$	Sparse label	“nose”, [0.45, 0.26, -0.18]
Mesh Recovery	Image	$\mathbf{x}_I$	Sparse label	[0.61, 0.42, 0.17] <sup>†</sup>
Skeleton-based Action	Sparse label	[[0.47, -0.21], [0.48, -0.20]...], “left knee”	Text	“kicking”

this line and further advances the field by simplifying heterogeneous representation across tasks into only two basic formats - continuous digits and discrete words. This simplification greatly enhances the flexibility and scalability of the model and enables our proposed Hulk to simultaneously address 2D vision, 3D vision, vision-language, and skeleton-based human-centric tasks without any task-specific adaptation.

### III. HUMAN-CENTRIC 2D VISION, 3D VISION, SKELETON-BASED AND VISION-LANGUAGE TASKS

Hulk, a *general human percevier*, is designed to handle a wide range of 2D vision, 3D vision, skeleton-based and vision-language tasks in a unified way. We collect vision, skeleton-based and multimodal datasets from 42 publicly available data sources as training datasets for our model. These datasets detailed in Sec. V-A1 cover 8 human-centric tasks.

The inputs and outputs of human-centric tasks can be categorized into 4 different modalities: *Images* - RGB images, whose normalized formulation is the matrix whose elements range between 0 and 1; *Texts* - Discrete words; *Sparse Labels* - the coordinates with its semantic meaning and locations, *e.g.*, “nose, [0.45, 0.26]”; *Dense labels* - per-pixel semantics represented by texts. In the following, we show that eight major human-centric tasks can be viewed as the translations among the four modalities. Examples are illustrated in Table II.

**Human Parsing & 2D Pose Estimation.** Given an image, human parsing and 2D pose estimation are required to generate the dense labels which are semantic segmentation maps for human parsing and keypoint heatmap for pose estimation<sup>2</sup>.

**Pedestrian Attribute Recognition & Image Caption.** The RGB images are projected into texts that describe their semantic meanings. For pedestrian attribution recognition, the output is the name of pedestrian attributes, while for the image caption, the output consists of sentences of discrete words as natural language descriptions of the image.

**Pedestrian Detection & 3D Pose Estimation & Human Mesh Recovery.** The RGB input images are projected to sparse labels, which include continuous digits to describe their locations and discrete words to describe its semantic meaning. For pedestrian detection, the sparse labels contain the location of the upper left point and bottom right point for bounding boxes and discrete words to describe the object class. For 3D pose estimation, the output is the 3D location of every

<sup>2</sup>In this paper, we leverage the heatmap-based methods for 2D pose estimation because we experimentally verify that heatmap-based methods generally achieve better performance than keypoint-regression-based methods.

keypoints and its class names, *e.g.*, noses and heads. For human mesh recovery, the output is only the 3D locations of mesh vertices defined in the SMPL model. Since these vertices do not have explicit semantic meaning, we do not predict the class name of every mesh vertex.

**Skeleton-based Action Recognition.** Given sparse labels that are a temporal sequence of keypoints with their semantic meaning and locations, the skeleton-based action recognition transforms the sparse labels to the texts of the action names.

### IV. HULK: A GENERAL HUMAN-CENTRIC KNOWLEDGE TRANSLATOR

We now introduce Hulk, a general human-centric knowledge translator, which can tackle human-centric 2D vision, 3D vision, skeleton-based, and vision-language tasks in one model without any task-specialist adaption. The key challenge is to unify the heterogeneous representations of the inputs and outputs. Our Hulk has two innovations to address the problem. First, our Hulk proposes that heterogeneous inputs and outputs can be unified into four different modalities, *i.e.*, texts, images, sparse labels (locations or location sequences) and dense labels (pixel-wise semantic words), which can be further simplified into two basic input and output formats of discrete semantic words and continuous values such as location coordinates. For instance, the pedestrian caption produces words that describe the appearance, age, dress-ups, *etc.*; the human parsing task predicts pixel-wise semantic words of the given image; the 3D pose estimation task predicts both the location of joints and their corresponding semantic words such as the nose and the right winkle. Second, our Hulk proposes a modality translation task where the major 2D vision, 3D vision, skeleton-based, and vision-language human-centric tasks can be viewed as its special case. The intuition of the modality translation task is that if a model well understands all human-centric knowledge, it only needs to translate from the input modality to the output modality, *e.g.*, human mesh recovery translates the image into sparse labels that are 3D location of mesh vertices, and skeleton-based action recognition translates the human keypoint temporal sequences into texts that describe the action semantic names.

#### A. Model Architecture

To realize the general modality translation for human-centric perceptions, our proposed Hulk, *i.e.*, *Human universal knowledge translator*, consists of three simple yet effective components: a modality-specialist tokenizer and de-tokenizer

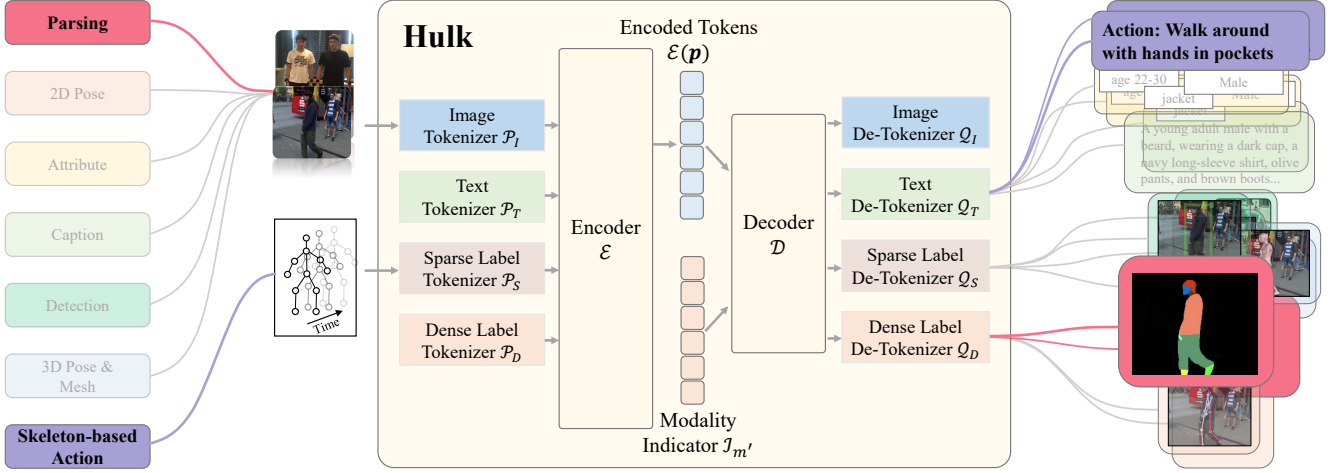


Fig. 2: The framework of our proposed Hulk. The pipeline for human parsing and skeleton-based action recognition tasks are highlighted in pink and purple. Given an input sample from the human parsing task, Hulk first tokenizes the image using the image tokenizer  $\mathcal{P}_I$  and sends tokens into the modality-shared encoder  $\mathcal{E}$  to learn general human-centric representations. Guided by the output modality indicator  $\mathcal{I}'_m$ , the decoder  $\mathcal{D}$  translates the encoded tokens to output tokens. Finally, the dense label de-tokenizer  $\mathcal{P}$  transforms output tokens into segmentation maps.

(Sec. IV-B) composed of two different heads to predict semantics and locations, a modality-agnostic encoder and decoder (Sec. IV-C) and a modality-specialist indicator (Sec. IV-C) to guide the modality-shared decoder to translate the features extracted by the encoder to the output modality. Finally, we leverage the contrastive loss to supervise the classification of semantic words and L1 loss to supervise the regression of locations. As shown in Fig. 2, the pipeline of our proposed Hulk of translating from the input modality to the output modality can be described as follows:

1) *Step1 – Tokenize modality-specific inputs into a modality-shared manifold space:* Given input data  $\mathbf{x}_m$  from one of the four modalities, *i.e.*, images  $I$ , texts  $T$ , sparse labels  $S$  and dense labels  $D$ , we leverage the modality-specialist tokenizer to project them into tokens  $\mathbf{p}$  in the modality-shared manifold, *i.e.*,  $\mathbf{p} = \mathcal{P}_m(\mathbf{x}_m)$ , where  $\mathcal{P}_m$  is the tokenizer of modality  $m$  before the transformer encoder  $\mathcal{E}$  and  $m \in \{I, T, S, D\}$  denotes the modality of input  $\mathbf{x}_m$ .

2) *Step2 – Translate the input tokens to the tokens of the output modality with the modality-shared encoder/decoder and the modality indicator for the decoder:* Given the input token  $\mathbf{p}$  and the output modality indicator  $\mathcal{I}'_m$ , we extract the human-centric representations by the encoder  $\mathcal{E}$ , and translate it into the output modality with the modality-shared decoder and the output modality indicator, *i.e.*, output tokens  $\mathbf{q} = \mathcal{D}(\mathcal{E}(\mathbf{p}), \mathcal{I}'_m)$ , where  $\mathcal{D}$  is the transformer decoder and  $m' \in \{I, T, S, D\}$  is the output modality.

3) *Step3 – Detokenize the output tokens after the decoder into the target modality and optimize the network with the contrastive loss for classifying the semantic words and L1 loss for regressing locations:* Given the translated tokens after the decoder, we generate the output modalities by the modality-specialist de-tokenizer, *i.e.*,  $\hat{\mathbf{y}}_s = \mathcal{Q}_s(\mathbf{q})$ . Finally, the parameters in the tokenizers  $\mathcal{P} \in \{\mathcal{P}_I, \mathcal{P}_T, \mathcal{P}_S, \mathcal{P}_D\}$ , the encoder  $\mathcal{E}$ , the decoder  $\mathcal{D}$ , the de-tokenizers  $\mathcal{Q} \in \{\mathcal{Q}_I, \mathcal{Q}_T, \mathcal{Q}_S, \mathcal{Q}_D\}$  and the modality indicators  $\mathcal{I}'_m \in \{\mathcal{I}_I, \mathcal{I}_T, \mathcal{I}_S, \mathcal{I}_D\}$  are optimized

by the contrastive loss for classifying semantic words and L1 loss for regressing locations.

### B. Tokenizer and De-Tokenizer

One of the most critical challenges to developing the *general human perceiver* is to tackle the heterogeneity of the inputs and outputs. While previous methods designed modality-specific projectors and task-specific heads to generate the diverse inputs and outputs, respectively, our Hulk proposes to tokenize task inputs and de-tokenize representations to task outputs in a simple interface: we only need to design two types of tokenizer and de-tokenizer blocks as shown in Fig. 3, *i.e.*, one to classify the semantic texts and the other to regress the locations, based on the intuition that the goal of perception tasks address is to recognize the semantic meaning and locate where it is. We further showcase these two types of blocks can be stacked to construct the tokenizers and de-tokenizers of four modalities in major human-centric tasks.

1) *Tokenizer and De-tokenizer Blocks:* Based on the observation that the goal of most perception tasks is to recognize the semantic meaning or to localize where the objects and keypoints are. Therefore, we design two pairs of tokenizers and de-tokenizers for classifying semantic words and regressing the digital locations, respectively.

**Semantic Tokenizer and De-tokenizer Block.** The semantic tokenizer block  $\mathcal{G}^s$  aims at tokenizing words in a modality-shared manifold, while the semantic de-tokenizer block  $\mathcal{H}^s$  aims at decoding the tokens to the words. The semantic tokenizer and de-tokenizer have dual designs. Specifically, given several words  $\mathbf{x}_w = \{\mathbf{x}_1^w, \mathbf{x}_2^w, \dots, \mathbf{x}_N^w\}$  representing different semantics, we extract the features<sup>3</sup>  $\mathbf{f}_w = \{\mathbf{f}_1^w, \mathbf{f}_2^w, \dots, \mathbf{f}_N^w\}$  by the off-shore BERT [63] model, where  $N$  is the number of

<sup>3</sup>According to the vocabulary of BERT, different words will be split into different number of tokens, leading to various lengths of extracted BERT features in different tasks. However, without loss of generality, we use the pooled BERT feature for all tasks.

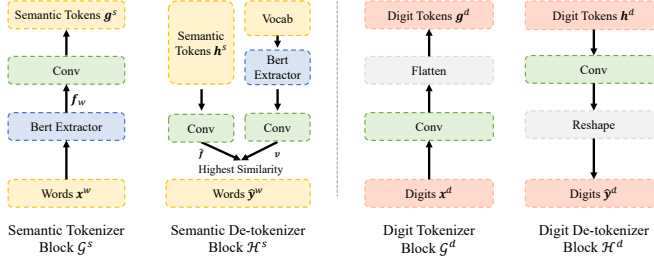


Fig. 3: Two tokenizer and de-tokenizer blocks. Semantic (de-)tokenizer classifies the semantics text and digit (de-)tokenizer regresses the locations.

words. In the skeleton-based action recognition task, semantics of joints are also introduced to enhance Hulk’s understanding of the movement of joints (please refer to Fig. 2). To emphasize the semantic correlation among nearing words, we use a convolutional network to generate the text tokens  $\mathbf{g}^s$ , *i.e.*,

$$\mathbf{g}^s = \mathcal{G}^s(\mathbf{x}_1^w, \mathbf{x}_2^w, \dots, \mathbf{x}_N^w) = \text{Conv}(\mathbf{f}_1^w, \mathbf{f}_2^w, \dots, \mathbf{f}_N^w), \quad (1)$$

where  $\mathbf{f}^i = \text{BERT}(\mathbf{x}_i^w)$  is the BERT feature of the word  $\mathbf{x}_i^w$ .

Accordingly, the semantic de-tokenizer block  $\mathcal{H}^s$  decodes the tokens to words. Given the words in the vocabulary, we extract the features of all words  $\mathbf{v} = \{\mathbf{v}_1, \mathbf{v}_2, \dots, \mathbf{v}_C\}$  by BERT and leverage the convolutional network to project the output semantic tokens  $\mathbf{h}^s$  to the BERT feature space  $\hat{\mathbf{f}}$ ,

$$\hat{\mathbf{f}} = \text{Conv}(\mathbf{h}^s). \quad (2)$$

Then we select the word  $\hat{\mathbf{y}}^w$  whose BERT feature is the most similar to the token feature, *i.e.*,

$$\hat{\mathbf{y}}^w = \mathcal{H}^s(\mathbf{h}^s, \mathbf{v}) = \{y_j = \text{argmax}_{k \in [1, C]} \mathbf{v}^\top \hat{\mathbf{f}}_j\}, j \in [1, N'], \quad (3)$$

where  $C$  and  $N'$  denote the number of semantic tokens in  $\mathbf{v}$  and output tokens, respectively.

**Digit Tokenizer and De-tokenizer Block.** The digit tokenizer  $\mathcal{G}^d$  and de-tokenizer block  $\mathcal{H}^d$  are designed for mutual conversion between continuous digits representing locations and tokens. Given the digit sequence  $\mathbf{x} = [\mathbf{x}_1, \mathbf{x}_2, \dots, \mathbf{x}_N]$ , where  $N$  is the length of digit sequence, we design the convolutional network to extract the information in the digits by transforming the digits to modality-shared tokens, and then flatten it into the token sequence, *i.e.*,

$$\mathbf{g}^d = \mathcal{G}^d([\mathbf{x}_1, \mathbf{x}_2, \dots, \mathbf{x}_N]) = \text{Flatten}(\text{Conv}([\mathbf{x}_1, \mathbf{x}_2, \dots, \mathbf{x}_N])). \quad (4)$$

Accordingly, to decode the digit tokens  $\mathbf{h}^d$  into digits indicating locations, we design the convolutional network to generate digits and then reshape the generated digits to the same shape as task outputs  $\hat{y}$ , *i.e.*,

$$\hat{y} = [\hat{y}_1, \hat{y}_2, \dots, \hat{y}_N'] = \mathcal{H}^d(\mathbf{h}^d) = \text{Reshape}(\text{Conv}(\mathbf{h}^d)), \quad (5)$$

where  $N'$  is the length of the output sequence.

2) *Stacking Blocks to Modality-specialist Tokenizers and De-tokenizers:* As detailed in Sec. III, we categorize the input and output formats of human-centric tasks into 4 different modalities: Text—sentences containing words; Image—RGB images; Sparse labels—a number of location coordinates in the image; Dense labels—per-pixel sentences to describe semantics.

**Image.** Most human-centric perception tasks rely on the image modality as inputs. An image  $\mathbf{x}_I \in \mathbb{R}^{C \times H \times W}$ , where  $C$  is the number of channels,  $H$  is the height of the image and  $W$  is the width of the image, is a matrix with continuous digits between 0 and 1 after normalization. Therefore, we directly leverage the digit tokenizer block  $\mathcal{G}^d$  as the image tokenizer, *i.e.*,

$$\mathbf{p} = \mathcal{P}_I(\mathbf{x}_I) = \mathcal{G}^d(\mathbf{x}_I), \quad (6)$$

where  $\mathbf{p}$  is the input tokens in the modality-shared manifold, and  $\mathcal{G}^d$  is the digit tokenizer block defined in Eq. 4. Since Hulk only focuses on human-centric perception tasks, we do not design an image de-tokenizer in this paper and leave it for future works.

**Text.** The text modality is the important output modality for human-centric perception tasks, including pedestrian caption, skeleton-based action recognition, *etc*. In practice, we directly leverage the semantic tokenizer block as the text tokenizer and the semantic de-tokenizer block as the text de-tokenizer. Given a text inputs of  $N$  words,  $\mathbf{x}_T = (\mathbf{x}_1^w, \mathbf{x}_2^w, \dots, \mathbf{x}_N^w)$ , with the text tokenizer, the input tokens  $\mathbf{p}$  can be computed by

$$\mathbf{p} = \mathcal{P}_T(\mathbf{x}_T) = \mathcal{G}^s(\mathbf{x}_1^w, \mathbf{x}_2^w, \dots, \mathbf{x}_N^w), \quad (7)$$

where  $\mathcal{G}^s$  is the semantic tokenizer block defined in Eq. 1.

For attribute or action classification tasks, to obtain the prediction words using the output token  $\mathbf{q}$ ,

$$\hat{\mathbf{y}}_T = \mathcal{Q}_T(\mathbf{q}) = \mathcal{H}(\mathbf{q}, \mathbf{v}), \quad (8)$$

where  $\mathcal{H}^s$  is the semantic de-tokenizer defined in Eq. 3,  $\mathbf{v}$  denotes the features of attribute or action classes.

For the pedestrian caption task, to auto-regressively decode the word  $\hat{\mathbf{y}}^w$  in task outputs  $\hat{\mathbf{y}}_T = (\hat{\mathbf{y}}_1^w, \hat{\mathbf{y}}_2^w, \dots, \hat{\mathbf{y}}_N^w)$ , we define the text de-tokenizer as

$$\hat{\mathbf{y}}_T = \mathcal{Q}_T(\mathbf{q}) = [\mathcal{H}^s(\mathbf{q}_1, \mathbf{v}), \mathcal{H}^s(\mathbf{q}_2, \mathbf{v}), \dots, \mathcal{H}^s(\mathbf{q}_N, \mathbf{v})], \quad (9)$$

where  $\mathbf{q}_i, i \in [1, N]$  denotes the  $i$ -th output tokens in auto-regressive manner,  $\mathbf{v}$  denotes the features of BERT vocabulary.

**Sparse Label.** The sparse labels usually refer to points with semantic meanings. For example, the task outputs of the pose estimation and task inputs of skeleton-based action recognition are the point coordinates and their corresponding semantic meanings. Therefore, the sparse label tokenizer and de-tokenizer combine semantic and digit blocks. We leverage the semantic block to encode the semantics of points and the digit blocks to encode the point locations. Specifically, given the sparse labels  $\mathbf{x}_S = (\mathbf{x}_S^s; \mathbf{x}_S^d)$ , where  $\mathbf{x}_S^s$  denotes the semantics of the sparse labels and  $\mathbf{x}_S^d$  denotes the digital locations of the sparse labels. Mathematically, the input tokens  $\mathbf{p}$  is computed using the sparse label tokenizer  $\mathcal{P}_S$  by

$$\mathbf{p} = \mathcal{P}_S(\mathbf{x}_S) = \mathcal{G}^s(\mathbf{x}_S^s) + \mathcal{G}^d(\mathbf{x}_S^d), \quad (10)$$

where  $\mathcal{G}^s$  and  $\mathcal{G}^d$  are the semantic tokenizer block (Eq. 1) and the digit tokenizer block (Eq. 4), respectively. Given the output tokens  $\mathbf{q}$  after the decoder, the sparse label de-tokenizer  $\mathcal{Q}_S$  decomposes it into semantics and digits of sparse label outputs  $\hat{\mathbf{y}}_S = (\hat{\mathbf{y}}_S^s, \hat{\mathbf{y}}_S^d)$ , where  $\hat{\mathbf{y}}_S^s$  and  $\hat{\mathbf{y}}_S^d$  are the semantics and digital locations of the output sparse label  $\hat{\mathbf{y}}_S$ . Specifically,

$$(\hat{\mathbf{y}}_S^s, \hat{\mathbf{y}}_S^d) = \mathcal{Q}_S(\mathbf{q}), \hat{\mathbf{y}}_S^s = \mathcal{H}^s(\mathbf{q}), \hat{\mathbf{y}}_S^d = \mathcal{H}^d(\mathbf{q}), \quad (11)$$

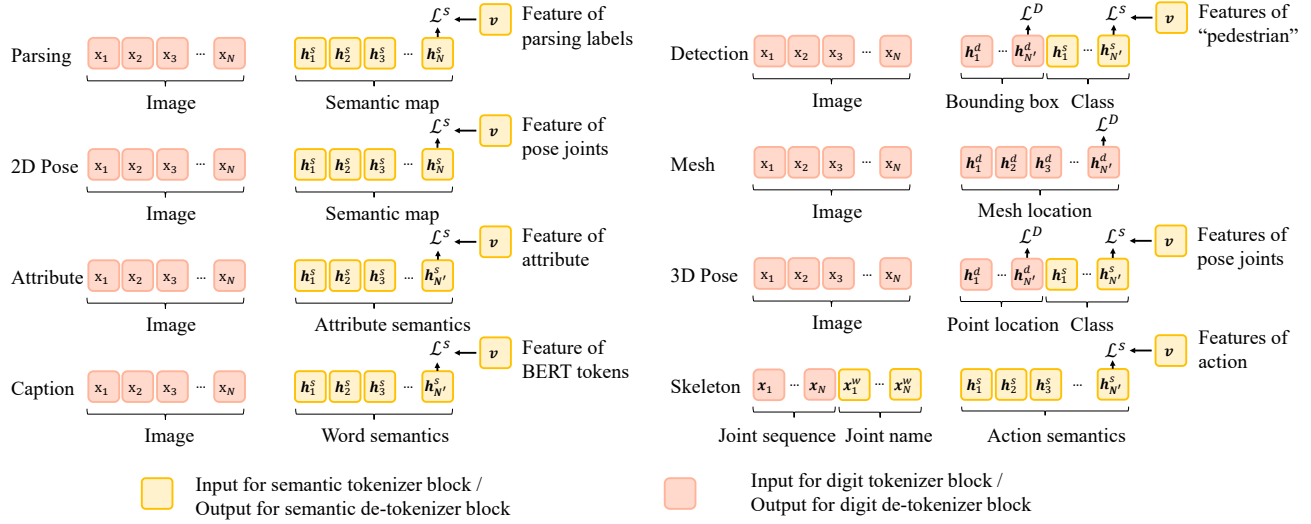


Fig. 4: Input, output tokens and objective functions for eight human-centric tasks. The objective function supervises all the output tokens while only one token’s loss is depicted here due to the limited space.

where  $\mathcal{H}^s$  and  $\mathcal{H}^d$  are the semantic de-tokenizer block (Eq. 3) and the digit de-tokenizer block (Eq. 5).

**Dense Label.** The dense labels are the semantic words for every pixel of the image. For the dense label tokenizer, given a dense label  $\mathbf{x}_D \in \mathbb{R}^{C \times H \times W}$ , where  $C$  is the number of classes consisting of different words, we leverage the semantic tokenizer block to transform it into input tokens  $\mathbf{p}$ , *i.e.*,

$$\mathbf{p} = \mathcal{P}_D(\mathbf{x}_D) = \mathcal{G}^s(\mathbf{x}_D). \quad (12)$$

Different from that in the text de-tokenizer, the decoder output  $\mathbf{q}$  often embeds the information of an image patch instead of a pixel. Therefore, the similarity is computed between the features of words in BERT vocabulary  $\mathbf{v}$  and the feature of upsampled output tokens  $\hat{\mathbf{f}}$  (Eq. 2). The dense label predictions are then computed by

$$\begin{aligned} \hat{\mathbf{y}}_D &= \mathcal{Q}_D(\mathbf{q}) \\ &= \{\hat{y}_j = \text{argmax}_{k \in [1, C]} \mathbf{v}^\top \text{Upsample}(\hat{\mathbf{f}}_j)\}, j \in [1, N'], \end{aligned} \quad (13)$$

where  $C$  denotes the different semantic classes in  $\mathbf{v}$ ,  $N'$  is the number of output tokens,  $\mathcal{Q}_D$  has the additional ‘‘Upsample’’ operator than  $\mathcal{H}^s$  defined Eq. 5.

### C. Token Translation

Given the modality-specific tokenizer and the modality-specific de-tokenizer, the encoder and the decoder translate the input tokens to output tokens with the guidance of the modality-specialist indicator. The design for token translation is similar to the architecture of ‘‘Transformer’’. Specifically, give the tokens  $\mathbf{p}$  of the input modality, the encoder extracts the general human-centric representations, and then the decoder translates the general representation to the output tokens  $\mathbf{q}$ , which is guided by the output modality indicator  $\mathcal{I}_{m'}$ . Mathematically, this process can be defined as

$$\mathbf{q} = \mathcal{D}(\mathcal{E}(\mathbf{p}), \mathcal{I}_{m'}), \quad (14)$$

where  $\mathcal{E}$  is the transformer encoder,  $\mathcal{D}$  is the transformer decoder, and  $\mathcal{I}_{m'} \in \mathbb{R}^{N' \times d_{out}}$ , where  $d_{out}$  is the dimension of decoder features,  $N'$  is the number of output tokens.

### D. Objective Functions

As illustrated in Sec. IV-B2, the modality-specific de-tokenizer will transform output tokens to the semantic part and the digital location part regarding corresponding human-centric tasks. Therefore, the diverse losses proposed in different human-centric tasks can be unified into two, *i.e.*, the contrastive loss to align the predicted semantics and the ground-truth labels, the digit regression loss to supervise the regressed point locations using the ground truth location.

1) *Semantic Contrastive Loss:* The semantic contrastive loss aims at aligning the predicted semantic words and the semantic labels of the text, the sparse label, and the dense label modality. Mathematically, given the conv-transformed features  $\hat{\mathbf{f}}$  of predicted semantic tokens  $\mathbf{h}^s$ , the BERT feature  $\mathbf{v}$  of the ground-truth semantic label containing the BERT features of all label candidates  $(\mathbf{v}_1, \mathbf{v}_2, \dots, \mathbf{v}_C)$ , the semantic contrastive loss is defined as

$$\mathcal{L}^s = \frac{\mathbf{v}_k^\top \hat{\mathbf{f}}}{\mathbf{v}_1^\top \hat{\mathbf{f}} + \mathbf{v}_2^\top \hat{\mathbf{f}} + \dots + \mathbf{v}_C^\top \hat{\mathbf{f}}}, \quad (15)$$

where  $k$  denotes the index of the selected semantic label in  $\mathbf{v}$  and the computation of  $\hat{\mathbf{f}}$  is defined in Eq. 2. Here,  $(\mathbf{v}_1, \mathbf{v}_2, \dots, \mathbf{v}_C)$  are the BERT features that differ in two types of tasks: classification tasks and caption tasks. For the classification task, *i.e.*, skeleton-based action recognition, attribute recognition, the candidate features are the BERT features of all class names in the defined task. For the caption task, *i.e.*, the pedestrian caption, the candidate features are the BERT features of all tokens in the BERT vocabulary.

2) *Digit Regression Loss:* The digit regression loss aims at predicting 3D coordinate values (3d pose estimation, human mesh recovery), or coordinate sequence values  $(x_1 y_1 x_2 y_2$

TABLE III  
STATISTICS OF TRAINING DATASETS.

Task type	Dataset	Number of samples
Human parsing (7 datasets)	Human3.6M [64]	
	LIP [65]	
	CIHP [66]	1,419,910
	...	
2D pose estimation (8 datasets)	COCO [67]	
	AIC [68]	
	Posetrack [69]	3,192,532
	...	
Attribute recognition (6 datasets)	RAPv2 [70]	
	PA100k [71]	
	parse27k [72]	10,911,029
	...	
Pedestrian detection (6 datasets)	CrowdHuman [73]	
	EuroCity [74]	
	WiderPerson [75]	170,687
	...	
Skeleton-based action (6 datasets)	Ntu60 [76]	
	GYM [77]	
	Diving48 [78]	391,685
	...	
Image caption (2 datasets)	CUHK-PEDS [79]	
	SYNTH-PEDES [80]	12,206,283
3D pose estimation (7 datasets)	Human3.6M [64]	
	Muco [81]	
Mesh recovery (7 datasets)	GTA [82]	1,895,710
	...	
Total	42	30,187,836 $\approx$ 30M

coordinates in pedestrian detection). Specifically, given the coordinates of the sparse labels, the digit regression is defined as

$$\mathcal{L}^d = Dis(\hat{\mathbf{y}}_S^d, \mathbf{y}_S^d), \quad (16)$$

where  $Dis(\hat{\mathbf{y}}_S^d, \mathbf{y}_S^d)$  measures the distance between predicted  $\hat{\mathbf{y}}_S^d$  and ground truth  $\mathbf{y}_S^d$ , which is different in different tasks, e.g., L1 loss and GIoU loss in the pedestrian detection.

3) *Overall Objective function*: In general multi-dataset learning of Hulk with  $K$  datasets, given the prediction  $\hat{\mathbf{y}}_i$  with ground truth  $\mathbf{y}_i, i = 1, 2, \dots, K$ , in  $i$ -th dataset, the overall objective function is defined as

$$\mathcal{L} = \sum_{i=1}^K \lambda_i \mathcal{L}_i(\hat{\mathbf{y}}_i, \mathbf{y}_i), \mathcal{L}_i \in \{\mathcal{L}^s, \mathcal{L}^d\}, \quad (17)$$

where  $\mathcal{L}_i$  is the dataset-specific loss with corresponding weight  $\lambda_i$ . For each task, we illustrate the input, output and the objective function in Fig. 4. Detailed losses for every human-centric task are elaborated in the supplementary material.

## V. EXPERIMENT

### A. Datasets and Evaluation Metric

1) *Training Datasets*: To establish a human-centric universal knowledge translator, we train the proposed Hulk at scale on a diverse and numerous collection of human-centric datasets. There are two major types of datasets: (1) datasets that leverage professional capture equipment [64], [83] or proficient human annotators [65]–[68], [70], [71], [73]. These

TABLE IV  
PEDESTRIAN DETECTION EVALUATION ON CROWDHUMAN [73] WITH mAP, MR<sup>-2</sup> AND JI. FOLLOWING UNIHCP [2], WE REPORT THE DIRECT EVAL AND FINE-TUNE (FT) RESULTS. †INDICATES USING A SMALLER INPUT RESOLUTION WITH A MAXIMUM HEIGHT/WIDTH OF 1120.

Method	Backbone	mAP	MR <sup>-2</sup> ↓	JI
Specialist	DETR [87]	ViT-B	75.9	73.2
	PEDR [88]	ViT-B	91.6	43.7
	DDETR [89]	ViT-B	91.5	43.7
	Sparse-RCNN [90]	ViT-B	91.3	44.8
	Iter-DDETR [37]	ViT-B	92.1	41.5
	Iter-Sparse-RCNN [37]	ViT-B	92.5	42.6
Iter-DDETR [37]	Swin-L	94.1	37.7	87.1
Pretraining	PATH [29]	ViT-B	90.9	-
	PATH [29]	ViT-L	90.8	-
Generalist	UniHCP [2]	ViT-B	90.0	46.6
	UniHCP-FT [2]	ViT-B	92.5	41.6
	Hulk	ViT-B	90.7	43.8
	Hulk-FT	ViT-B	92.4	40.7
	Hulk	ViT-L	92.2	40.1
	Hulk-FT	ViT-L	93.0	36.5

datasets generally provide supervision in high quality but are less scalable due to high costs. (2) pseudo-annotated datasets [6], [80] whose annotations are generated by state-of-the-art methods [84], [85]. Although the annotations of these data are not of high quality, they can greatly enrich the scenarios of the training data, of which the effectiveness has been proven by existing work [80], [86]. Generally, 42 publically available datasets are gathered to form the training set for Hulk, containing 30,187,836 training samples and covering eight different human-centric tasks – human parsing, 2D pose estimation, attribute recognition, pedestrian detection, skeleton-based action recognition, image caption, 3D pose estimation, and mesh recovery. Table III presents the number of datasets and samples in each task. Following the de-duplication practice in UniHCP [2], we remove the samples that could appear in the evaluation datasets. More detailed dataset setups can be found in the supplementary.

2) *Evaluation Datasets*: To evaluate the performance of Hulk across diverse human-centric tasks, following UniHCP [2], we select multiple core datasets to form a comprehensive benchmark. Specifically, CrowdHuman [73] is selected for evaluation on pedestrian detection, COCO [67] and AIC [68] are selected for 2D pose estimation, Human3.6M [64], LIP [65] and CIHP [66] are selected for human parsing, PA-100K [71] and RAPv2 [70] are selected for attribute recognition. Additionally, Caltech [91], MPII [92], ATR [93], and PETA [94] are also included to evaluate the transferability of Hulk.

For newly included tasks, we use the most widely-used benchmarks, *i.e.*, 3DPW [83] and Human3.6M [64] for 3D pose estimation and mesh recovery, NTU60-XSUB [76] for skeleton-based action recognition, CUHK-PEDES [79] for image caption on pedestrians.

### B. Implementation Details

Following UniHCP [2] and PATH [29], we use the standard ViT-Base [95] as the default backbone and initialize

TABLE V

2D POSE ESTIMATION EVALUATION ON COCO [67] VAL SET AND ON AIC [68] TEST SET WITH MAP. WE COMPARE OUR METHOD WITH OTHER SOTA METHODS, BOTH SPECIALISTS AND GENERALISTS, WITH AN INPUT RESOLUTION OF  $256 \times 192$ .  $\dagger$ INDICATES THE IMPLEMENTATION.  $\ddagger$ INDICATES THAT MULTIPLE DATASETS ARE USED.

Method	Backbone	COCO	AIC
Specialist	HRNet [99]	HRNet-W32	74.4
	HRNet [99]	HRNet-W48	75.1
	TokenPose-L/D24 [100]	HRNet-W48	75.8
	HRFormer-B [35]	HRFormer-B	75.6
	ViTPose-B [36]	ViT-B	75.8
	ViTPose-B $\ddagger$ [36]	ViT-B	77.1
	ViTPose++-B $\ddagger$ [101]	ViT-B	77.0
	ViTPose-L [36]	ViT-L	78.3
	ViTPose-L $\ddagger$ [36]	ViT-L	78.7
	ViTPose++-L $\ddagger$ [101]	ViT-L	78.6
Pretraining	HCMoCo $\dagger$ [62]	HRNet-W48	76.9
	SOLDIER [28]	Swin-B	76.6
	HAP [30]	ViT-B	77.0
	PATH [29]	ViT-B	76.3
	PATH [29]	ViT-L	77.1
Generalist	UniHCP [2]	ViT-B	76.1
	UniHCP-FT [2]	ViT-B	76.6
	Hulk	ViT-B	77.0
	Hulk-FT	ViT-B	77.5
	Hulk	ViT-L	78.3
	Hulk-FT	ViT-L	78.7
			37.1

it with unsupervised MAE pretraining [96]. Unless otherwise specified, the input resolution is consistent within each task, *i.e.*,  $256 \times 192$  resolution for 2D pose estimation and attribute recognition,  $480 \times 480$  resolution for human parsing,  $224 \times 224$  resolution for 3D pose estimation and mesh recovery,  $17 \text{ joints} \times 175$  frames for skeleton-based action recognition,  $384 \times 384$  resolution for image caption, and a maximum height/width of 1120 for pedestrian detection. Due to the high GPU memory demand of detection tasks, we resize the maximum height/width of the input images from the commonly used 1333 to 1120, which has a certain impact on the performance of detection tasks but does not affect the superiority of Hulk over other methods.

Considering the computational and communication efficiency during training, we adopt the practices in UniHCP to run one specific task on each GPU with gradient checkpointing [97]. We use the same Adafactor optimizer as that in UniHCP with  $\beta_1 = 0.9$ ,  $\beta_2$  clipped at 0.999 and disable the parameter scaling. We adopt a 60000-iteration schedule with a linear warm-up for the first 2000 iterations. We set the base learning rate to  $10^{-3}$  with a cosine decay scheduler. For ViT-B backbone, we use a drop-path-rate of 0.2, a layer-wise learning rate decay of 0.75, and set weight decay to 0.05. We also train the ViT-L with a drop-path-rate of 0.5, a layer-wise learning rate decay of 0.85, and a weight decay of 0.1, following the recommendation setup in ViTDET [98]. To better utilize the knowledge in every dataset, we do not restrict that all datasets should take the same epoch during training and provide detailed joint training setup in the supplementary. The whole training takes 70, 144 hours in total on 80 NVIDIA A100 GPUS for ViT-B, ViT-L, respectively.

TABLE VI

HUMAN PARSING EVALUATION ON HUMAN3.6M [64], LIP [65] AND CIHP [66] WITH MIoU. WE COMPARE OUR METHOD WITH OTHER SOTA METHODS, INCLUDING SPECIALISTS, GENERALISTS, AND PRETRAININGS, WITH AN INPUT RESOLUTION OF  $480 \times 480$ .  $\dagger$ INDICATED THE RE-IMPLEMENTATION.

Method	Backbone	H3.6M	LIP	CIHP
Specialist	SNT [102]	ResNet-101	-	54.73
	PCNet [103]	ResNet-101	-	57.03
	SCHP [84]	ResNet-101	-	59.36
	CDGNet [104]	ResNet-101	-	60.30
Pretraining	HCMoCo [62]	HRNet-18	62.50	-
	HCMoCo $\dagger$ [62]	HRNet-48	66.01	-
	SOLDIER [28]	Swin-B	-	60.50
	PATH [29]	ViT-B	65.00	61.40
Generalist	PATH [29]	ViT-L	66.20	62.60
	UniHCP [2]	ViT-B	65.90	63.80
	UniHCP-FT [2]	ViT-B	65.95	63.86
	Hulk	ViT-B	68.08	63.95
	Hulk-FT	ViT-B	68.56	63.98
	Hulk	ViT-L	69.31	65.86
	Hulk-FT	ViT-L	69.89	66.02
				72.68

### C. Comparison with States-of-the-art Methods

Extensive evaluations are conducted to demonstrate the capabilities of our Hulk across diverse human-centric tasks. Table IV-IX show the experimental results of Hulk on eight different human-centric tasks, *i.e.*, pedestrian detection, 2D pose estimation, human parsing, pedestrian attribute recognition, 3D human pose and mesh recovery, skeleton-based action recognition, and pedestrian image caption.

To facilitate a more detailed analysis, we categorize the comparative methods into three distinct classes: (1) Specialist models, referring to models custom-tailored specifically for the target task; (2) Pretraining models, involving models pre-trained on datasets distinct from the target task, followed by fine-tuning on the target task; and (3) Generalist models, which are designed as unified frameworks capable of handling multiple tasks simultaneously.

Following the practice in UniHCP, we report two kinds of evaluation results of our Hulk: (1) **direct evaluation**, where the pre-trained model are directly used for evaluation on the target dataset, and (2) **finetuning**, where the pretrained Hulk are first finetuned with the train split of the target dataset and then evaluated.

*1) 2D Vision Tasks:* As observed, our proposed Hulk demonstrates promising performance on four 2D vision tasks, *i.e.*, pedestrian detection, 2D pose estimation, human parsing, and pedestrian attribute recognition.

**Pedestrian detection.** In the pedestrian detection task,  $MR^{-2}$  is employed as a more sensitive and crucial metric in detection in the crowd scenes. This metric is particularly sensitive to False Positives (FP), with lower values indicating more desirable performance. We use an input image resolution of a maximum height/weight of 1120, while other methods take a large resolution of 1333 by default. As shown in Table IV, Hulk showcases competitive performance with State-Of-The-Art (SOTA) using a smaller input resolution. Specifically, after finetuning, our Hulk achieves an improvement of **-0.7%**

TABLE VII  
PEDESTRIAN ATTRIBUTE RECOGNITION EVALUATION ON PA-100K [71]  
AND RAPV2 [70] WITH MA REPORTED.

Method	Backbone	PA-100K	RAPV2
Specialist	SSC [105]	ResNet-50	81.87
	C-Tran [106]	ResNet-101	81.53
	Q2L [107]	TResNetL	80.72
	L2L [108]	ViT-B	82.24
	DAFL [109]	ResNet-50	83.54
Pretraining	SOLDIER [28]	Swin-B	86.37
	HAP [30]	ViT-B	86.54
	PATH [29]	ViT-B	86.90
	PATH [29]	ViT-L	90.80
Generalist	UniHCP [2]	ViT-B	79.32
	UniHCP-FT [2]	ViT-B	86.18
	Hulk	ViT-B	82.85
	Hulk-FT	ViT-B	<b>87.85</b>
	Hulk	ViT-L	84.36
	Hulk-FT	ViT-L	88.97
			85.86

MR<sup>-2</sup> on ViT-B and **-1.2% MR<sup>-2</sup>** on ViT-L, respectively, compared to SOTA specialist methods, *e.g.*, Iter-DDETR [37].

**2D pose estimation.** To evaluate the performance of Hulk on 2D pose estimation task, we conduct evaluations on both the COCO and AIC datasets. The results are listed in Table V. Hulk model improves previous SOTA by considerable margins on AIC, *i.e.*, **+0.6%** AP and **+0.8%** on ViT-B and ViT-L, respectively. The performance gain demonstrates the good scalability of Hulk. Hulk achieves on-par performance compared with ViTPose++ [101] on COCO. We attribute the relatively small performance gain on COCO to the distribution gap between the training subset and evaluation subset, where models are trained with on ground-truth boxes but evaluated on estimated boxes with a detector obtaining human AP of 56 on COCO valset [110].

**Human parsing.** We evaluate the performance of Hulk on the human parsing task on Human3.6M, LIP, and CIHP datasets. As shown in Table VI, when using ViT-B, Hulk surpasses SOTA methods by **+2.36%** mIoU, **+1.46%** mIoU on Human3.6M and CIHP, respectively. On LIP, although Hulk achieves a relatively small performance gain with ViT-B, Hulk showcases considerable performance with ViT-B, *i.e.*, 66.02% mIoU, demonstrating excellent scalability of Hulk.

**Pedestrian attribute recognition.** We evaluate the performance of our Hulk on PA-100K and RAPV2 datasets to demonstrate its effectiveness on the pedestrian attribute recognition task. Results are listed in Table VII. As can be seen, on ViT-B, Hulk outperforms previous methods by obtaining 87.85% mA and 85.26% mA on PA-100K and RAPV2, respectively. The performance of the large Hulk with ViT-B further increases to 88.97% mA and 85.86% mA, showing competitive results without adopting task-specific heads in human-centric pretraining models [29].

2) **Skeleton-based Tasks:** In the **skeleton-based action recognition** task, existing methods utilize three categories of backbones: (1) Graph Convolutional Networks (GCN), which are the most common architecture; (2) Convolutional Neural Networks (CNN) and Recurrent Neural Networks (RNN), and (3) more recently, Transformer architectures. Our Hulk falls

TABLE VIII  
SKELETON-BASED ACTION RECOGNITION EVALUATION ON NTU60-XSUB [112] WITH ACCURACY RESULTS REPORTED.

Method	Backbone	Accuracy
Specialist	ST-GCN [113]	81.5
	AS-GCN [114]	86.8
	AGCN [115]	88.5
	Shift-GCN [116]	90.7
	CrosSCLR [117]	86.2
	MCC [118]	89.7
	SCC [119]	88.0
	UNIK [120]	86.8
	CTR-GCN [121]	92.4
	MS-G3D [122]	91.5
	IndRNN [123]	81.8
	MTCNN [124]	81.1
Generalist	HCN [125]	86.5
	PoseConv3D [111]	93.1
	ST-TR [126]	89.9
	DSTA-Net [127]	91.5
Pretraining	STTFormer [128]	89.9
	MotionBERT [1]	DSTformer
	Hulk	ViT-B
	Hulk-FT	ViT-B
Generalist	Hulk	ViT-L
	Hulk-FT	ViT-L

TABLE IX  
PEDESTRIAN IMAGE CAPTAIN EVALUATION ON CUHK-PEDES [79].

Model	Backbone	B@4	CIDEr
Specialist	BLIP [129]	ViT-B	32.9
	BLIP-2 [51]	ViT-B	32.8
Generalist	Hulk	ViT-B	31.1
	Hulk-FT	ViT-B	28.3
	Hulk	ViT-L	31.6
	Hulk-FT	ViT-L	30.5

within the third category. To assess the effectiveness of Hulk, we report results on NTU60-XSub, a well-known dataset on skeleton-based action recognition. The results in Table VIII indicate that even without specific pretraining designs [1], Hulk obtains a remarkable accuracy of **93.8%** on ViT-B, better than the SOTA PoseConv3D [111] method. After finetuning Hulk with ViT-L backbone, the performance on NTU60-XSub further increases to **94.3%**. This improvement not only highlights the effectiveness of Hulk in the skeleton-based action recognition, but also demonstrates Hulk’s ability of tokenizing skeleton and image inputs into a modality-shared manifold space to extract generalized human-centric knowledge.

3) **Vision-language Tasks:** We also evaluate Hulk on the CUHK-PEDES dataset for the vision-language task, *i.e.*, **pedestrian image caption**. For fair comparisons, we reimplemented the state-of-the-art BLIP [129] and BLIP-2 [51] methods by finetuning its pre-trained weights (on a 129M image-text dataset) on the CUHK-PEDES dataset. As shown in Table IX, Hulk achieves on-par performance with BLIP and BLIP-2 on the B@4 metric but lags behind in terms of CIDEr. This discrepancy in performance can be attributed to

TABLE X  
MONOCULAR 3D HUMAN POSE AND MESH RECOVERY EVALUATION ON 3DPW [83] AND HUMAN3.6M [64] AMONG IMAGE-BASED METHODS.

Method	Backbone	3DPW			Human3.6M	
		MPVPE $\downarrow$	MPJPE $\downarrow$	PA-MPJPE $\downarrow$	MPJPE $\downarrow$	PA-MPJPE $\downarrow$
Specialist	HMR [131]	ResNet-50	-	130.0	76.7	88.0
	GraphCMR [132]	ResNet-50	-	-	70.2	-
	SPIN [133]	ResNet-50	116.4	96.9	59.2	62.5
	I2LMeshNet [134]	ResNet-50	-	93.2	57.7	55.7
	PyMAF [135]	ResNet-50	110.1	92.8	58.9	57.7
	ROMP [136]	ResNet-50	105.6	89.3	53.5	-
	ROMP [136]	HRNet-W32	103.1	85.5	53.3	-
	PARE [137]	ResNet-50	99.7	82.9	52.3	-
	METRO [138]	ResNet-50	-	-	-	56.5
	METRO [138]	HRNet-W64	88.2	77.1	47.9	54.0
	PARE [137]	HRNet-W32	88.6	74.5	46.5	-
	MeshGraphomer [139]	HRNet-W64	87.7	74.7	45.6	51.2
	ProHMR [140]	ResNet-50	-	-	59.8	-
	OCHMR [141]	ResNet-50	107.1	89.7	58.3	-
	3DCrowdNet [142]	ResNet-50	98.3	81.7	51.5	-
	FastMETRO [143]	ResNet-50	90.6	77.9	48.3	53.9
	FastMETRO [143]	HRNet-W64	84.1	73.5	44.6	52.2
Pretraining	CLIFF [130]	ResNet-50	81.2	69.0	43.0	47.1
	VisDB [144]	ResNet-50	85.5	73.5	44.9	51.0
Generalist	MotionBERT [1]	DSTformer	88.1	76.9	47.2	53.8
	HAP [30]	ViT-B	90.1	56.0	106.3	-
	Hulk	ViT-B	79.8	67.0	39.9	43.6
	Hulk-FT	ViT-B	80.7	68.9	41.3	44.9
	Hulk	ViT-L	77.4	66.3	38.5	40.3
	Hulk-FT	ViT-L	79.9	68.3	40.6	41.4

the extensive pretraining of BLIP and BLIP-2 on large-scale vision-language datasets, while our Hulk is trained solely on smaller human-centric vision-language datasets (about 12M). Furthermore, we observed that finetuning on the CUHK-PEDES dataset led to a decline in the model’s prediction accuracy, because better pedestrian captions can learn from diverse annotations in large-scale human-centric datasets.

**4) 3D Vision Tasks:** In the case of the 3D vision task, *i.e.*, **3D human pose estimation and mesh recovery**, our Hulk improves the previous state-of-the-art method CLIFF [130], by **-3.8** MPVPE, **-2.7** MPJPE, **-4.5** PA-MPJPE on 3DPW dataset, and **-6.8** MPJPE, **-3.9** PA-MPJPE on Human3.6M dataset, in direct evaluation scenarios. Interestingly, comparing with direct evaluation results, we observed that finetuning on both 3DPW and Human3.6M datasets will lead to lower performances, showing the effectiveness of pretraining our Hulk on diverse tasks.

#### D. Ablation Study

To demonstrate the effectiveness of Hulk, we conduct several ablations on a smaller training set. The ablation set consists of 21 datasets with about 1.7M samples, covering all eight tasks. We provide the detailed dataset combination in the supplementary. Without otherwise specified, we train Hulk for 20k iterations in all ablation variants. While results on different datasets within the same task are highly related, we showcase one dataset per task to represent the performance on the specific task in the main text (all results are provided in the supplementary material). As the metric in 3D pose estimation and mesh recovery computes the error, we use  $100 - \text{error}$  when we need to compute average performance among 8 tasks.

**1) Weight sharing:** As Hulk demonstrates promising performance in various human-centric tasks while sharing mostly all parameters, we explore the impact of incorporating more task-specific parameters into our learning framework. To assess the effectiveness of our weight-sharing approach, we ablate three weight-sharing variants: (a) Our Hulk model, all parameters in both the encoder and decoder are shared across all datasets, and parameters in the tokenizers and de-tokenizers are shared within the same input/output modality. (b) All parameters in both the encoder and decoder are shared across all datasets, but the parameters in the tokenizers and de-tokenizers are dataset-specific. (c) Only encoder parameters are shared. In Table XI, we observed that more parameter sharing enhances the overall performance of the model. Specifically, introducing decoder parameter sharing (from (b) to (c)) significantly benefits task performances by **+12.1%** on average. This shows that human-centric tasks require shared human semantic information in different human-related annotations. A notable example is the skeleton-based action recognition task. When only the encoder parameters are shared, the model fails to converge, resulting in only **1.7%** accuracy on the NTU60-XSub dataset. However, by sharing more model parameters, the general knowledge from other tasks substantially is beneficial to better accuracy in this task.

**2) Task Collaboration and Interference:** In this section, we explore how various human-centric tasks influence each other. We conduct leave-one-out experiments that we remove one task from our training set every time (as detailed in Table XII). Notably, mesh recovery and 3D pose estimation were always conducted together. We compare these scenarios against a baseline to determine if omitting a task would positively or

TABLE XI

COMPARISON OF DIFFERENT PARAMETER-SHARING SCHEMES.  $\mathcal{E}$ ,  $\mathcal{D}$ ,  $\mathcal{P}$ , AND  $\mathcal{Q}$  DENOTE ENCODER, DECODER, TOKENIZER, AND DE-TOKENIZER, RESPECTIVELY. WITH MORE TASK-SPECIFIC PARAMETERS, THE AVERAGE TASKS PERFORMANCE OF HULK DECLINE SIGNIFICANTLY.

Methods	Shared module				Parsing	2D Pose	Detection	Attribute	Caption	Skeleton	Mesh	3D Pose	Avg
	$\mathcal{E}$	$\mathcal{D}$	$\mathcal{P}$	$\mathcal{Q}$	LIP	AIC	CrowdHuman	RAPv2	CUHK-PEDES	NTU60-Sub	3DPW	3DPW	
					mIoU	AP	AP	mA	B@4	Acc	100-MPVPE	100-MPJPE	
(a) Hulk	✓	✓	✓	✓	56.8	25.5	81.8	77.9	28.0	93.2	-0.3	13.2	41.8
(b)	✓	✓			56.8	25.8	80.6	78.8	26.7	93.8	-3.0	10.7	41.1
(c)	✓				56.3	25.7	75.9	81.3	28.7	1.7	-11.2	2.9	29.0

TABLE XII

ALABTION OF COLLABORATION AND INTERFERENCE BETWEEN TASKS. IN GREEN AND RED ARE THE GAPS OF AT LEAST  $\pm 0.5$  POINTS.

Method	Parsing	2D Pose	Detection	Attribute	Caption	Skeleton	Mesh	3D Pose	Avg.
	LIP	AIC	CrowdHuman	RAPv2	CUHK-PEDES	NTU60-Sub	3DPW	3DPW	
	mIoU	AP	AP	mA	B@4	Acc	100-MPVPE	100-MPJPE	
baseline	56.8	25.5	81.8	77.9	28.0	93.2	-0.3	13.2	-
w/o Parsing	-	25.2 <sup>0.3</sup>	78.5 <sup>3.3</sup>	77.3 <sup>0.6</sup>	25.8 <sup>2.2</sup>	93.2 <sup>0.0</sup>	-2.9 <sup>2.6</sup>	10.8 <sup>2.4</sup>	-1.6
w/o 2D Pose	52.3 <sup>4.5</sup>	-	65.0 <sup>16.8</sup>	75.1 <sup>2.8</sup>	26.6 <sup>1.5</sup>	93.5 <sup>0.3</sup>	-18.9 <sup>18.6</sup>	-3.5 <sup>16.7</sup>	-8.6
w/o Detection	57.6 <sup>0.8</sup>	26.4 <sup>0.9</sup>	-	77.6 <sup>0.3</sup>	27.8 <sup>0.2</sup>	93.1 <sup>0.1</sup>	-4.8 <sup>4.5</sup>	10.5 <sup>2.7</sup>	-0.9
w/o Attribute	56.9 <sup>0.1</sup>	25.6 <sup>0.1</sup>	79.9 <sup>1.9</sup>	-	28.2 <sup>0.2</sup>	93.1 <sup>0.1</sup>	-2.1 <sup>1.8</sup>	13.2 <sup>1.0</sup>	-0.6
w/o Caption	57.3 <sup>0.5</sup>	25.6 <sup>0.1</sup>	80.2 <sup>1.6</sup>	77.8 <sup>0.1</sup>	-	92.9 <sup>0.3</sup>	-2.2 <sup>1.9</sup>	11.2 <sup>2.0</sup>	-0.8
w/o Skeleton	57.4 <sup>0.6</sup>	25.7 <sup>0.2</sup>	80.9 <sup>0.9</sup>	77.4 <sup>0.5</sup>	28.2 <sup>0.2</sup>	-	-4.8 <sup>4.5</sup>	9.9 <sup>3.3</sup>	-1.2
w/o Mesh&3D Pose	57.4 <sup>0.6</sup>	25.5 <sup>0.0</sup>	81.0 <sup>0.8</sup>	78.0 <sup>0.1</sup>	27.9 <sup>0.1</sup>	93.1 <sup>0.1</sup>	-	-	-0.1

negatively impact the performance of others.

We observe several key findings. First, removing any task generally leads to lower average performance of human-centric tasks. Particularly, removing the 2D Pose task significantly decreased performance in detection (**-16.8 AP**), mesh recovery (increased error by **18.6 MPVPE**), and 3D pose estimation (increased error by **16.7 MPJPE**). We consider that the pose information in 2D is highly important to that in 3D and can help the model perceive the boundary of pedestrians, making the 2D pose estimation task essential in training a human-centric foundation model. Second, tasks such as the performances of pedestrian detection, mesh recovery, and 3D pose estimation are more sensitive to the removal of other tasks. Their performance markedly declined, indicating a high interdependence among these human-centric tasks during training. Third, skeleton-based action recognition was less affected by the absence of other tasks, which may stem from its unique input type (skeleton points) compared to the image-based input of other tasks. It is also worth noting that the absence of certain tasks resulted in performance gains for human parsing, indicating potential task conflicts with other human-centric tasks that require further investigation.

3) *Attention Mask Designs in the Decoder*: The receptive field of the attention module in the decoder is crucial for the translation and de-tokenization of features in the unified model. Therefore, we investigate the effects of different attention masks as illustrated in Fig. 5: (a) our Hulk model adopts task-specialized attention masks for different tasks, i.e., for pose estimation and mesh recovery tasks, we employ full attention; for parsing, detection, attribute, and skeleton-based tasks, we use diagonal attention; for caption tasks, we apply a combination of causal and diagonal attention. We also experimented with (b) all tasks using full attention and (c) all tasks using diagonal attention. The results, shown in Table XIII,

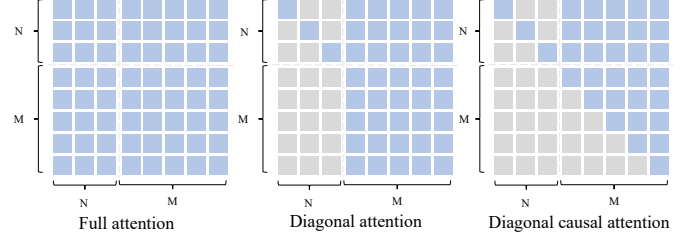


Fig. 5: Given  $N$  encoded tokens  $\mathcal{E}(\mathbf{p})$  with  $M$  modality indicators  $\mathcal{I}_s$ , we proposed various attention mask in the decoder  $\mathcal{D}$  to facilitate diverse tasks. **Left:** Full attention enables comprehensive interaction between encoder tokens and modality indicators. **Mid:** Diagonal attention mitigates potential distortions in encoded tokens due to randomly initialized modality indicators. **Right:** A combination of the causal and diagonal masks for image captioning.

indicate that employing different attention interaction methods for different tasks can improve the performances, *i.e.*, **+0.4%** and **+1.0%** average performance gain on full attention and diagonal attention, respectively.

4) *Scaling up data size*: To assess the impact of the diverse and sufficient human-centric data, we train Hulk using a longer 60000-iteration schedule on the ablation datasets comprising 1.7M training samples, and full datasets comprising 30M training samples, respectively. Results in Table XIV indicate that incorporating more human-centric data brings considerable performance improvement across all tasks, with notable enhancements in 2D pose estimation (**+2.3% AP**), pedestrian detection (**+1.6% AP**), image caption (**+2.1 B@4**), mesh recovery (**-26.0 MPVPE**) and 3D pose estimation (**-24.5 MPJPE**). Slight improvements are also noted in attribute recognition and skeleton-based action recognition. We attribute these modest gains to the lower quality of data and the significant domain gap in the extended datasets. For instance, in attribute recognition, we include LU-Person [6] with its pseudo labels that offers less informative supervision compared to

TABLE XIII  
COMPARISON OF DIFFERENT ATTENTION MASKS.

Methods	Parsing		2D Pose		Detection		Attribute		Caption		Skeleton		Mesh		3D Pose		Avg	
	LIP		AIC		CrowdHuman		RAPv2		CUHK-PEDES		NTU60-Sub		3DPW		3DPW			
	mIoU	AP	AP	mA	B@4	Acc	100-MPVPE	100-MPJPE										
(a) Hulk	56.8	25.5	81.8	77.9	28.0	93.2	-0.3	13.2	47.0									
(b) full-attn	57.2	25.4	79.9	77.6	28.6	91.8	-1.0	13.4	46.6									
(c) diag-attn	56.6	25.6	80.3	78.0	28.4	93.1	-4.1	10.0	46.0									

TABLE XIV

PERFORMANCE OF HULK ON DIVERSE HUMAN-CENTRIC TASKS WHEN SCALING UP DATA SIZE. EXPERIMENTS ARE BOTH TRAINED WITH A **FULL 60,000-ITERATION SCHEDULE**, SHOWING THAT LEARN FROM ADDITIONAL DATA AND ACHIEVE BETTER PERFORMANCE ON AVERAGE.

Data samples	Parsing		2D Pose		Detection		Attribute		Caption		Skeleton		Mesh		3D Pose		Avg.	
	LIP		AIC		CrowdHuman		RAPv2		CUHK-PEDES		NTU60-Sub		3DPW		3DPW			
	mIoU	AP	AP	mA	B@4	Acc	100-MPVPE	100-MPJPE										
1.7M	63.5	32.2	89.1	80.8	29.0	93.7	-5.8	8.5	48.9									
30M	64.0	34.5	90.7	80.9	31.1	93.8	20.2	33.0	56.0									

TABLE XV  
COMPARISON OF DIFFERENT INITIALIZATION PARAMETERS.

Methods	Parsing		2D Pose		Detection		Attribute		Caption		Skeleton		Mesh		3D Pose		Avg	
	LIP		AIC		CrowdHuman		RAPv2		CUHK-PEDES		NTU60-Sub		3DPW		3DPW			
	mIoU	AP	AP	mA	B@4	Acc	100-MPVPE	100-MPJPE										
(a) MAE [96]	56.8	25.5	81.8	77.9	28.0	93.2	-0.3	13.2	47.2									
(b) HAP [30]	63.3	33.4	85.4	81.8	29.6	91.5	9.6	22.9	52.2									
(c) PATH [29]	63.6	34.5	88.6	80.2	29.9	92.8	8.3	21.3	52.4									

other training datasets. Similarly, the Kinetics-400 dataset, which has a substantial domain gap from NTU60, influences the results for the skeleton-based action recognition.

5) *Different initialization weights*: To examine the influence of model initialization on performance, we conduct additional experiments using pre-training parameters from the human-centric models, *i.e.*, HAP [30] and PATH [29], and compare them with our baseline Hulk initialized by MAE [96]. The results, detailed in Table XV, indicate that initializing Hulk with parameters from human-centric pretraining methods can further enhance its accuracy. This result not only validates the robustness of Hulk but also highlight its potential for further enhancement. Moreover, it is important to note that for a fair comparison with other human-centric models, we refrain from using these specialized pretraining parameters as our default initialization method in main results, ensuring the improvement observed in Hulk are attributed to its novel architecture and learning strategy.

## VI. CONCLUSION AND LIMITATIONS

In this paper, we introduce Hulk, a novel general human-centric perceiver that marks the first integration of major 2D and 3D vision tasks, skeleton-based models, and vision-language tasks into a unified framework. Diverging from traditional models that rely on task-specific heads, Hulk adopts an innovative approach by decomposing these into two basic heads, thereby enhancing adaptability and simplifying the process. Trained on extensive datasets, Hulk not only achieves state-of-the-art performance across various tasks but does so without the need for dataset-specific fine-tuning. Beyond the

success in human-centric tasks, we also shed light on the essential components for developing a human-centric foundation model. Hulk represents a significant step for human-centric foundation models, offering a versatile and effective framework that paves the way for advanced research.

**Potential Negatives Impacts.** As a foundation model for human-centric tasks, Hulk's extensive data requirements and prolonged training time raise concerns about environmental impact due to high energy consumption. To mitigate this, future research should focus on improving computational efficiency. Additionally, Hulk is trained and evaluated on several human-centric datasets, thus may contain biases in these datasets, which need continuous effort to address to ensure ethical application.

**Limitations.** Currently, the scope and the capabilities of Hulk is limited by resource constraints and training costs, preventing further exploration of other human-centric tasks, *e.g.*, 3D human generation. Overcoming these barriers remains a lot of future work and will enable us to fully realize the theoretical potential of Hulk. Despite the limitations, Hulk stands as a pioneering framework in human-centric foundation models, offering a glimpse into the future where such models are more inclusive and efficient.

## ACKNOWLEDGEMENTS

This work is supported by the National Key R&D Program of China(NO.2022ZD0160100), National Natural Science Foundation of China (No.62127803), and Key R&D Project of Zhejiang Province (No.2022C01056)

## REFERENCES

- [1] Wentao Zhu, Xiaoxuan Ma, Zhaoyang Liu, Libin Liu, Wayne Wu, and Yizhou Wang. Motionbert: A unified perspective on learning human motion representations. In *Proceedings of the IEEE/CVF International Conference on Computer Vision*, pages 15085–15099, 2023.
- [2] Yuanzheng Ci, Yizhou Wang, Meilin Chen, Shixiang Tang, Lei Bai, Feng Zhu, Rui Zhao, Fengwei Yu, Donglian Qi, and Wanli Ouyang. Unihep: A unified model for human-centric perceptions. In *Proceedings of the IEEE/CVF Conference on Computer Vision and Pattern Recognition*, pages 17840–17852, 2023.
- [3] Xiatian Zhu, Botong Wu, Dongcheng Huang, and Wei-Shi Zheng. Fast open-world person re-identification. *IEEE Transactions on Image Processing*, 27(5):2286–2300, 2017.
- [4] Ruibing Hou, Bingpeng Ma, Hong Chang, Xinqian Gu, Shiguang Shan, and Xilin Chen. Feature completion for occluded person re-identification. *IEEE Transactions on Pattern Analysis and Machine Intelligence*, 44(9):4894–4912, 2021.
- [5] Xiaokang Zhang, Yan Yan, Jing-Hao Xue, Yang Hua, and Hanzi Wang. Semantic-aware occlusion-robust network for occluded person re-identification. *IEEE Transactions on Circuits and Systems for Video Technology*, 31(7):2764–2778, 2020.
- [6] Dengpan Fu, Dongdong Chen, Jianmin Bao, Hao Yang, Lu Yuan, Lei Zhang, Houqiang Li, and Dong Chen. Unsupervised pre-training for person re-identification. In *Proceedings of the IEEE/CVF conference on computer vision and pattern recognition*, pages 14750–14759, 2021.
- [7] Gregory Rogez, Philippe Weinzaepfel, and Cordelia Schmid. Lcrnet++: Multi-person 2d and 3d pose detection in natural images. *IEEE transactions on pattern analysis and machine intelligence*, 42(5):1146–1161, 2019.
- [8] Yi Yang and Deva Ramanan. Articulated human detection with flexible mixtures of parts. *IEEE transactions on pattern analysis and machine intelligence*, 35(12):2878–2890, 2012.
- [9] Tao Yu, Zerong Zheng, Kaiwen Guo, Jianhui Zhao, Qionghai Dai, Hao Li, Gerard Pons-Moll, and Yebin Liu. Doublefusion: Real-time capture of human performances with inner body shapes from a single depth sensor. In *Proceedings of the IEEE conference on computer vision and pattern recognition*, pages 7287–7296, 2018.
- [10] Hao-Shu Fang, Jiefeng Li, Hongyang Tang, Chao Xu, Haoyi Zhu, Yuliang Xiu, Yong-Lu Li, and Cewu Lu. Alphapose: Whole-body regional multi-person pose estimation and tracking in real-time. *IEEE Transactions on Pattern Analysis and Machine Intelligence*, 2022.
- [11] Matthew Loper, Naureen Mahmood, Javier Romero, Gerard Pons-Moll, and Michael J Black. Smpl: A skinned multi-person linear model. In *Seminal Graphics Papers: Pushing the Boundaries, Volume 2*, pages 851–866. 2023.
- [12] Javier Fernández, Luke Bornn, and Dan Cervone. Decomposing the immeasurable sport: A deep learning expected possession value framework for soccer. In *13th MIT Sloan Sports Analytics Conference*, 2019.
- [13] Tom Decroos, Lotte Bransen, Jan Van Haaren, and Jesse Davis. Actions speak louder than goals: Valuing player actions in soccer. In *Proceedings of the 25th ACM SIGKDD international conference on knowledge discovery & data mining*, pages 1851–1861, 2019.
- [14] Yutaro Honda, Rei Kawakami, Ryota Yoshihashi, Kenta Kato, and Takeshi Naemura. Pass receiver prediction in soccer using video and players' trajectories. In *Proceedings of the IEEE/CVF Conference on Computer Vision and Pattern Recognition*, pages 3503–3512, 2022.
- [15] Mohammad Zahrawi and Khaled Shaalan. Improving video surveillance systems in banks using deep learning techniques. *Scientific Reports*, 13(1):7911, 2023.
- [16] Ratnesh Litoriya, Dev Ramchandani, Dhruvansh Moyal, and Dhruv Bothra. Integrated and deep learning-based social surveillance system: a novel approach. *Journal of Automation, Mobile Robotics and Intelligent Systems*, 16(3):30–39, 2022.
- [17] Sangeeta Yadav, Preeti Gulia, Nasib Singh Gill, Jyotir Moy Chatterjee, et al. A real-time crowd monitoring and management system for social distance classification and healthcare using deep learning. *Journal of Healthcare Engineering*, 2022, 2022.
- [18] Tieqi Shou, Zuhuan Ye, Yayao Hong, Zhiyuan Wang, Hang Zhu, Zhihan Jiang, Dingqi Yang, Binbin Zhou, Cheng Wang, and Longbiao Chen. Crowdq: Predicting the queue state of hospital emergency department using crowdsensing mobility data-driven models. *Proceedings of the ACM on Interactive, Mobile, Wearable and Ubiquitous Technologies*, 7(3):1–28, 2023.
- [19] Mohamed Khalil, Christoph Bergs, Theodoros Papadopoulos, Roland Wüchner, Kai-Uwe Bletzinger, and Michael Heizmann. Iiot-based fatigue life indication using augmented reality. In *2019 IEEE 17th International Conference on Industrial Informatics (INDIN)*, volume 1, pages 746–751, 2019.
- [20] Kaiyuan Hu, Haowen Yang, Yili Jin, Junhua Liu, Yongting Chen, Miao Zhang, and Fangxin Wang. Understanding user behavior in volumetric video watching: Dataset, analysis and prediction. In *Proceedings of the 31st ACM International Conference on Multimedia*, pages 1108–1116, 2023.
- [21] Wang Zhen, Tang Dunbing, Liu Changchun, Xiong Xin, Zhang Linqi, Zhang Zhuocheng, and Liu Xuan. Augmented-reality-assisted bearing fault diagnosis in intelligent manufacturing workshop using deep transfer learning. In *2021 Global Reliability and Prognostics and Health Management (PHM-Nanjing)*, pages 1–6. IEEE, 2021.
- [22] Zhuo Su, Lan Xu, Dawei Zhong, Zhong Li, Fan Deng, Shuxue Quan, and Lu Fang. Robustfusion: Robust volumetric performance reconstruction under human-object interactions from monocular rgbd stream. *IEEE Transactions on Pattern Analysis and Machine Intelligence*, 45(5):6196–6213, 2022.
- [23] Yao-Chih Lee, Ji-Ze Genevieve Jang, Yi-Ting Chen, Elizabeth Qiu, and Jia-Bin Huang. Shape-aware text-driven layered video editing. In *Proceedings of the IEEE/CVF Conference on Computer Vision and Pattern Recognition (CVPR)*, pages 14317–14326, June 2023.
- [24] Gyeongman Kim, Hajin Shim, Hyunsu Kim, Yunjey Choi, Junho Kim, and Eunho Yang. Diffusion video autoencoders: Toward temporally consistent face video editing via disentangled video encoding. In *Proceedings of the IEEE/CVF Conference on Computer Vision and Pattern Recognition (CVPR)*, pages 6091–6100, June 2023.
- [25] Sanyi Zhang, Xiaochun Cao, Guo-Jun Qi, Zhanjie Song, and Jie Zhou. Aiparsing: anchor-free instance-level human parsing. *IEEE Transactions on Image Processing*, 31:5599–5612, 2022.
- [26] Ziwei Zhang, Chi Su, Liang Zheng, Xiaodong Xie, and Yuan Li. On the correlation among edge, pose and parsing. *IEEE Transactions on Pattern Analysis and Machine Intelligence*, 44(11):8492–8507, 2021.
- [27] Xiaodan Liang, Liang Lin, Wei Yang, Ping Luo, Junshi Huang, and Shuicheng Yan. Clothes co-parsing via joint image segmentation and labeling with application to clothing retrieval. *IEEE Transactions on Multimedia*, 18(6):1175–1186, 2016.
- [28] Weihua Chen, Xianzhe Xu, Jian Jia, Hao Luo, Yaohua Wang, Fan Wang, Rong Jin, and Xiuyu Sun. Beyond appearance: a semantic controllable self-supervised learning framework for human-centric visual tasks. In *Proceedings of the IEEE/CVF Conference on Computer Vision and Pattern Recognition*, pages 15050–15061, 2023.
- [29] Shixiang Tang, Cheng Chen, Qingsong Xie, Meilin Chen, Yizhou Wang, Yuanzheng Ci, Lei Bai, Feng Zhu, Haiyang Yang, Li Yi, et al. Humanbench: Towards general human-centric perception with projector assisted pretraining. In *Proceedings of the IEEE/CVF Conference on Computer Vision and Pattern Recognition*, pages 21970–21982, 2023.
- [30] Junkun Yuan, Xinyu Zhang, Hao Zhou, Jian Wang, Zhongwei Qiu, Zhiyin Shao, Shaofeng Zhang, Sifan Long, Kun Kuang, Kun Yao, et al. Hap: Structure-aware masked image modeling for human-centric perception. *arXiv preprint arXiv:2310.20695*, 2023.
- [31] Zhongang Cai, Wanqi Yin, Ailing Zeng, Chen Wei, Qingping Sun, Yanjun Wang, Hui En Pang, Haiyi Mei, Mingyuan Zhang, Lei Zhang, et al. Smpler-x: Scaling up expressive human pose and shape estimation. *arXiv preprint arXiv:2309.17448*, 2023.
- [32] OpenAI. OpenAI: Introducing ChatGPT, 2022.
- [33] InternLM Team. Internlm: A multilingual language model with progressively enhanced capabilities, 2023.
- [34] Jie Zhou, Ganqu Cui, Shengding Hu, Zhengyan Zhang, Cheng Yang, Zhiyuan Liu, Lifeng Wang, Changcheng Li, and Maosong Sun. Graph neural networks: A review of methods and applications. *AI open*, 1:57–81, 2020.
- [35] Yuhui Yuan, Rao Fu, Lang Huang, Weihong Lin, Chao Zhang, Xilin Chen, and Jingdong Wang. Hrformer: High-resolution vision transformer for dense predict. *Advances in Neural Information Processing Systems*, 34:7281–7293, 2021.
- [36] Yufei Xu, Jing Zhang, Qiming Zhang, and Dacheng Tao. Vitpose: Simple vision transformer baselines for human pose estimation. *arXiv preprint arXiv:2204.12484*, 2022.
- [37] Anlin Zheng, Yuang Zhang, Xiangyu Zhang, Xiaojuan Qi, and Jian Sun. Progressive end-to-end object detection in crowded scenes. In *Proceedings of the IEEE/CVF Conference on Computer Vision and Pattern Recognition*, pages 857–866, 2022.

[38] Biao Zhang, Deyi Xiong, and Jinsong Su. Neural machine translation with deep attention. *IEEE transactions on pattern analysis and machine intelligence*, 42(1):154–163, 2018.

[39] Ashish Vaswani, Noam Shazeer, Niki Parmar, Jakob Uszkoreit, Llion Jones, Aidan N Gomez, Łukasz Kaiser, and Illia Polosukhin. Attention is all you need. *Advances in neural information processing systems*, 30, 2017.

[40] Alec Radford, Jong Wook Kim, Chris Hallacy, Aditya Ramesh, Gabriel Goh, Sandhini Agarwal, Girish Sastry, Amanda Askell, Pamela Mishkin, Jack Clark, et al. Learning transferable visual models from natural language supervision. In *International conference on machine learning*, pages 8748–8763. PMLR, 2021.

[41] Hu Xu, Gargi Ghosh, Po-Yao Huang, Dmytro Okhonko, Armen Aghajanyan, Florian Metze, Luke Zettlemoyer, and Christoph Feichtenhofer. Videoclip: Contrastive pre-training for zero-shot video-text understanding. *arXiv preprint arXiv:2109.14084*, 2021.

[42] Andrey Guzhov, Federico Raue, Jörn Hees, and Andreas Dengel. Audioclip: Extending clip to image, text and audio. In *ICASSP 2022-2022 IEEE International Conference on Acoustics, Speech and Signal Processing (ICASSP)*, pages 976–980. IEEE, 2022.

[43] Rohit Girdhar, Alaaeldin El-Nouby, Zhuang Liu, Mannat Singh, Kalyan Vasudev Alwala, Armand Joulin, and Ishan Misra. Imagebind: One embedding space to bind them all. In *Proceedings of the IEEE/CVF Conference on Computer Vision and Pattern Recognition*, pages 15180–15190, 2023.

[44] Honghui Yang, Sha Zhang, Di Huang, Xiaoyang Wu, Haoyi Zhu, Tong He, Shixiang Tang, Hengshuang Zhao, Qibo Qiu, Binbin Lin, et al. Unipad: A universal pre-training paradigm for autonomous driving. *arXiv preprint arXiv:2310.08370*, 2023.

[45] Honghui Yang, Tong He, Jiaheng Liu, Hua Chen, Boxi Wu, Binbin Lin, Xiaofei He, and Wanli Ouyang. Gd-mae: generative decoder for mae pre-training on lidar point clouds. In *Proceedings of the IEEE/CVF Conference on Computer Vision and Pattern Recognition*, pages 9403–9414, 2023.

[46] Roman Bachmann, David Mizrahi, Andrei Atanov, and Amir Zamir. Multimae: Multi-modal multi-task masked autoencoders. In *European Conference on Computer Vision*, pages 348–367. Springer, 2022.

[47] Gukyeong Kwon, Zhaowei Cai, Avinash Ravichandran, Erhan Bas, Rahul Bhotika, and Stefano Soatto. Masked vision and language modeling for multi-modal representation learning. *arXiv preprint arXiv:2208.02131*, 2022.

[48] Yuanze Lin, Chen Wei, Huiyu Wang, Alan Yuille, and Cihang Xie. Smaug: Sparse masked autoencoder for efficient video-language pre-training. In *Proceedings of the IEEE/CVF International Conference on Computer Vision*, pages 2459–2469, 2023.

[49] Zhenfei Yin, Jiong Wang, Jianjian Cao, Zhelun Shi, Dingning Liu, Mukai Li, Lu Sheng, Lei Bai, Xiaoshui Huang, Zhiyong Wang, et al. Lamm: Language-assisted multi-modal instruction-tuning dataset, framework, and benchmark. *arXiv preprint arXiv:2306.06687*, 2023.

[50] Keqin Chen, Zhao Zhang, Weili Zeng, Richong Zhang, Feng Zhu, and Rui Zhao. Shikra: Unleashing multimodal llm’s referential dialogue magic. *arXiv preprint arXiv:2306.15195*, 2023.

[51] Junnan Li, Dongxu Li, Silvio Savarese, and Steven Hoi. Blip-2: Bootstrapping language-image pre-training with frozen image encoders and large language models. *arXiv preprint arXiv:2301.12597*, 2023.

[52] Haotian Liu, Chunyuan Li, Qingyang Wu, and Yong Jae Lee. Visual instruction tuning. *arXiv preprint arXiv:2304.08485*, 2023.

[53] Bo Li, Yuanhan Zhang, Liangyu Chen, Jinghao Wang, Jingkang Yang, and Ziwei Liu. Otter: A multi-modal model with in-context instruction tuning. *arXiv preprint arXiv:2305.03726*, 2023.

[54] Yan Zeng, Hanbo Zhang, Jiani Zheng, Jiangnan Xia, Guoqiang Wei, Yang Wei, Yuchen Zhang, and Tao Kong. What matters in training a gpt4-style language model with multimodal inputs? *arXiv preprint arXiv:2307.02469*, 2023.

[55] Yixuan Su, Tian Lan, Huayang Li, Jialu Xu, Yan Wang, and Deng Cai. Pandapgpt: One model to instruction-follow them all. *arXiv preprint arXiv:2305.16355*, 2023.

[56] Runsen Xu, Xiaolong Wang, Tai Wang, Yilun Chen, Jiangmiao Pang, and Dahua Lin. Pointllm: Empowering large language models to understand point clouds. *arXiv preprint arXiv:2308.16911*, 2023.

[57] Le Xue, Mingfei Gao, Chen Xing, Roberto Martín-Martín, Jiajun Wu, Caiming Xiong, Ran Xu, Juan Carlos Niebles, and Silvio Savarese. Ulip: Learning a unified representation of language, images, and point clouds for 3d understanding. In *Proceedings of the IEEE/CVF Conference on Computer Vision and Pattern Recognition*, pages 1179–1189, 2023.

[58] Josh Gardner, Simon Durand, Daniel Stoller, and Rachel M Bittner. Llark: A multimodal foundation model for music. *arXiv preprint arXiv:2310.07160*, 2023.

[59] Edward J Hu, Yelong Shen, Phillip Wallis, Zeyuan Allen-Zhu, Yuanzhi Li, Shean Wang, Lu Wang, and Weizhu Chen. Lora: Low-rank adaptation of large language models. *arXiv preprint arXiv:2106.09685*, 2021.

[60] Renrui Zhang, Jiaming Han, Aojun Zhou, Xiangfei Hu, Shilin Yan, Pan Lu, Hongsheng Li, Peng Gao, and Yu Qiao. Llama-adapter: Efficient fine-tuning of language models with zero-init attention. *arXiv preprint arXiv:2303.16199*, 2023.

[61] Haoyi Zhu, Honghui Yang, Xiaoyang Wu, Di Huang, Sha Zhang, Xianglong He, Tong He, Hengshuang Zhao, Chunhua Shen, Yu Qiao, et al. Ponderv2: Pave the way for 3d foundataion model with a universal pre-training paradigm. *arXiv preprint arXiv:2310.08586*, 2023.

[62] Fangzhou Hong, Liang Pan, Zhongang Cai, and Ziwei Liu. Versatile multi-modal pre-training for human-centric perception. In *Proceedings of the IEEE/CVF Conference on Computer Vision and Pattern Recognition*, pages 16156–16166, 2022.

[63] Jacob Devlin, Ming-Wei Chang, Kenton Lee, and Kristina Toutanova. Bert: Pre-training of deep bidirectional transformers for language understanding. *arXiv preprint arXiv:1810.04805*, 2018.

[64] Catalin Ionescu, Dragos Papava, Vlad Olaru, and Cristian Sminchisescu. Human3.6m: Large scale datasets and predictive methods for 3d human sensing in natural environments. *IEEE Transactions on Pattern Analysis and Machine Intelligence*, 36(7):1325–1339, jul 2014.

[65] Ke Gong, Xiaodan Liang, Dongyu Zhang, Xiaohui Shen, and Liang Lin. Look into person: Self-supervised structure-sensitive learning and a new benchmark for human parsing. In *Proceedings of the IEEE conference on computer vision and pattern recognition*, pages 932–940, 2017.

[66] Ke Gong, Xiaodan Liang, Yicheng Li, Yimin Chen, Ming Yang, and Liang Lin. Instance-level human parsing via part grouping network. In *Proceedings of the European conference on computer vision (ECCV)*, pages 770–785, 2018.

[67] Tsung-Yi Lin, Michael Maire, Serge Belongie, James Hays, Pietro Perona, Deva Ramanan, Piotr Dollár, and C Lawrence Zitnick. Microsoft coco: Common objects in context. In *Computer Vision–ECCV 2014: 13th European Conference, Zurich, Switzerland, September 6–12, 2014, Proceedings, Part V 13*, pages 740–755. Springer, 2014.

[68] Jiahong Wu, He Zheng, Bo Zhao, Yixin Li, Baoming Yan, Rui Liang, Wenjia Wang, Shipei Zhou, Guosen Lin, Yanwei Fu, et al. Large-scale datasets for going deeper in image understanding. In *2019 IEEE International Conference on Multimedia and Expo (ICME)*, pages 1480–1485. IEEE, 2019.

[69] Mykhaylo Andriluka, Umar Iqbal, Eldar Insafutdinov, Leonid Pishchulin, Anton Milan, Juergen Gall, and Bernt Schiele. Posetrack: A benchmark for human pose estimation and tracking. In *Proceedings of the IEEE conference on computer vision and pattern recognition*, pages 5167–5176, 2018.

[70] Dangwei Li, Zhang Zhang, Xiaotang Chen, and Kaiqi Huang. A richly annotated pedestrian dataset for person retrieval in real surveillance scenarios. *IEEE transactions on image processing*, 28(4):1575–1590, 2019.

[71] Xihui Liu, Haiyu Zhao, Maoqing Tian, Lu Sheng, Jing Shao, Shuai Yi, Junjie Yan, and Xiaogang Wang. Hydraplus-net: Attentive deep features for pedestrian analysis. In *Proceedings of the IEEE international conference on computer vision*, pages 350–359, 2017.

[72] Patrick Sudowe, Hannah Spitzer, and Bastian Leibe. Person Attribute Recognition with a Jointly-trained Holistic CNN Model. In *ICCV’15 ChaLearn Looking at People Workshop*, 2015.

[73] Shuai Shao, Zijian Zhao, Boxun Li, Tete Xiao, Gang Yu, Xiangyu Zhang, and Jian Sun. Crowdhuman: A benchmark for detecting human in a crowd. *arXiv preprint arXiv:1805.00123*, 2018.

[74] Markus Braun, Sebastian Krebs, Fabian Flohr, and Dariu M Gavrila. The eurocity persons dataset: A novel benchmark for object detection. *arXiv preprint arXiv:1805.07193*, 2018.

[75] Shifeng Zhang, Yiliang Xie, Jun Wan, Hansheng Xia, Stan Z Li, and Guodong Guo. Widerperson: A diverse dataset for dense pedestrian detection in the wild. *IEEE Transactions on Multimedia*, 22(2):380–393, 2019.

[76] Amit Shahroudy, Jun Liu, Tian-Tsong Ng, and Gang Wang. Ntu rgb+d: A large scale dataset for 3d human activity analysis. In *Proceedings of the IEEE conference on computer vision and pattern recognition*, pages 1010–1019, 2016.

[77] Dian Shao, Yue Zhao, Bo Dai, and Dahua Lin. Finegym: A hierarchical video dataset for fine-grained action understanding. In *Proceedings of*

the IEEE/CVF conference on computer vision and pattern recognition, pages 2616–2625, 2020.

[78] Yingwei Li, Yi Li, and Nuno Vasconcelos. Resound: Towards action recognition without representation bias. In *Proceedings of the European Conference on Computer Vision (ECCV)*, pages 513–528, 2018.

[79] Shuang Li, Tong Xiao, Hongsheng Li, Bolei Zhou, Dayu Yue, and Xiaogang Wang. Person search with natural language description. In *Proceedings of the IEEE conference on computer vision and pattern recognition*, pages 1970–1979, 2017.

[80] Jialong Zuo, Changqian Yu, Nong Sang, and Changxin Gao. Plip: Language-image pre-training for person representation learning. *arXiv preprint arXiv:2305.08386*, 2023.

[81] Dushyant Mehta, Oleksandr Sotnychenko, Franziska Mueller, Weipeng Xu, Srinath Sridhar, Gerard Pons-Moll, and Christian Theobalt. Single-shot multi-person 3d pose estimation from monocular rgb. In *2018 International Conference on 3D Vision (3DV)*, pages 120–130. IEEE, 2018.

[82] Zhongang Cai, Mingyan Zhang, Jiawei Ren, Chen Wei, Daxuan Ren, Zhengyu Lin, Haiyu Zhao, Lei Yang, Chen Change Loy, and Ziwei Liu. Playing for 3d human recovery. *arXiv preprint arXiv:2110.07588*, 2021.

[83] Timo von Marcard, Roberto Henschel, Michael Black, Bodo Rosenhahn, and Gerard Pons-Moll. Recovering accurate 3d human pose in the wild using imus and a moving camera. In *European Conference on Computer Vision (ECCV)*, sep 2018.

[84] Peike Li, Yunqiu Xu, Yunchao Wei, and Yi Yang. Self-correction for human parsing. *IEEE Transactions on Pattern Analysis and Machine Intelligence*, 2020.

[85] Alec Radford, Jeffrey Wu, Rewon Child, David Luan, Dario Amodei, Ilya Sutskever, et al. Language models are unsupervised multitask learners. *OpenAI blog*, 1(8):9, 2019.

[86] Alexander Kirillov, Eric Mintun, Nikhila Ravi, Hanzi Mao, Chloe Rolland, Laura Gustafson, Tete Xiao, Spencer Whitehead, Alexander C Berg, Wan-Yen Lo, et al. Segment anything. *arXiv preprint arXiv:2304.02643*, 2023.

[87] Nicolas Carion, Francisco Massa, Gabriel Synnaeve, Nicolas Usunier, Alexander Kirillov, and Sergey Zagoruyko. End-to-end object detection with transformers. In *European conference on computer vision*, pages 213–229. Springer, 2020.

[88] Matthieu Lin, Chuming Li, Xingyuan Bu, Ming Sun, Chen Lin, Junjie Yan, Wanli Ouyang, and Zhidong Deng. Detr for crowd pedestrian detection. *arXiv preprint arXiv:2012.06785*, 2020.

[89] Xizhou Zhu, Weijie Su, Lewei Lu, Bin Li, Xiaogang Wang, and Jifeng Dai. Deformable detr: Deformable transformers for end-to-end object detection. *arXiv preprint arXiv:2010.04159*, 2020.

[90] Peize Sun, Rufeng Zhang, Yi Jiang, Tao Kong, Chenfeng Xu, Wei Zhan, Masayoshi Tomizuka, Lei Li, Zehuan Yuan, Changhu Wang, et al. Sparse r-cnn: End-to-end object detection with learnable proposals. In *Proceedings of the IEEE/CVF conference on computer vision and pattern recognition*, pages 14454–14463, 2021.

[91] Piotr Dollar, Christian Wojek, Bernt Schiele, and Pietro Perona. Pedestrian detection: An evaluation of the state of the art. *IEEE transactions on pattern analysis and machine intelligence*, 34(4):743–761, 2011.

[92] Mykhaylo Andriluka, Leonid Pishchulin, Peter Gehler, and Bernt Schiele. 2d human pose estimation: New benchmark and state of the art analysis. In *Proceedings of the IEEE Conference on computer Vision and Pattern Recognition*, pages 3686–3693, 2014.

[93] Xiaodan Liang, Chunyan Xu, Xiaohui Shen, Jianchao Yang, Si Liu, Jinhui Tang, Liang Lin, and Shuicheng Yan. Human parsing with contextualized convolutional neural network. In *Proceedings of the IEEE international conference on computer vision*, pages 1386–1394, 2015.

[94] Yubin Deng, Ping Luo, Chen Change Loy, and Xiaou Tang. Pedestrian attribute recognition at far distance. In *Proceedings of the 22nd ACM international conference on Multimedia*, pages 789–792, 2014.

[95] Alexey Dosovitskiy, Lucas Beyer, Alexander Kolesnikov, Dirk Weissenborn, Xiaohua Zhai, Thomas Unterthiner, Mostafa Dehghani, Matthias Minderer, Georg Heigold, Sylvain Gelly, et al. An image is worth 16x16 words: Transformers for image recognition at scale. *arXiv preprint arXiv:2010.11929*, 2020.

[96] Kaiming He, Xinlei Chen, Saining Xie, Yanghao Li, Piotr Dollár, and Ross Girshick. Masked autoencoders are scalable vision learners. In *Proceedings of the IEEE/CVF conference on computer vision and pattern recognition*, pages 16000–16009, 2022.

[97] Elvis Rojas, Albert Njoroge Kahira, Esteban Meneses, Leonardo Bautista Gomez, and Rosa M Badia. A study of checkpointing in large scale training of deep neural networks. *arXiv preprint arXiv:2012.00825*, 2020.

[98] Yanghao Li, Hanzi Mao, Ross Girshick, and Kaiming He. Exploring plain vision transformer backbones for object detection. In *European Conference on Computer Vision*, pages 280–296. Springer, 2022.

[99] Ke Sun, Bin Xiao, Dong Liu, and Jingdong Wang. Deep high-resolution representation learning for human pose estimation. In *Proceedings of the IEEE/CVF conference on computer vision and pattern recognition*, pages 5693–5703, 2019.

[100] Yanjie Li, Shoukui Zhang, Zhicheng Wang, Sen Yang, Wankou Yang, Shu-Tao Xia, and Erjin Zhou. Tokenpose: Learning keypoint tokens for human pose estimation. In *Proceedings of the IEEE/CVF International Conference on Computer Vision*, pages 11313–11322, 2021.

[101] Yufei Xu, Jing Zhang, Qiming Zhang, and Dacheng Tao. Vitpose++: Vision transformer for generic body pose estimation. *IEEE Transactions on Pattern Analysis and Machine Intelligence*, 2023.

[102] Ruyi Ji, Dawei Du, Libo Zhang, Longyin Wen, Yanjun Wu, Chen Zhao, Feiyue Huang, and Siwei Lyu. Learning semantic neural tree for human parsing. In *European Conference on Computer Vision*, pages 205–221. Springer, 2020.

[103] Xiaomei Zhang, Yingying Chen, Bingke Zhu, Jinqiao Wang, and Ming Tang. Part-aware context network for human parsing. In *Proceedings of the IEEE/CVF Conference on Computer Vision and Pattern Recognition*, pages 8971–8980, 2020.

[104] Kunliang Liu, Ouk Choi, Jianming Wang, and Wonjun Hwang. Cdgnnet: Class distribution guided network for human parsing. In *Proceedings of the IEEE/CVF Conference on Computer Vision and Pattern Recognition*, pages 4473–4482, 2022.

[105] Jian Jia, Xiaotang Chen, and Kaiqi Huang. Spatial and semantic consistency regularizations for pedestrian attribute recognition. In *Proceedings of the IEEE/CVF international conference on computer vision*, pages 962–971, 2021.

[106] Jack Lanchantin, Tianlu Wang, Vicente Ordonez, and Yanjun Qi. General multi-label image classification with transformers. *arXiv preprint arXiv:2011.14027*, 2020.

[107] Shilong Liu, Lei Zhang, Xiao Yang, Hang Su, and Jun Zhu. Query2label: A simple transformer way to multi-label classification. *arXiv preprint arXiv:2107.10834*, 2021.

[108] Wanhua Li, Zhexuan Cao, Jianjiang Feng, Jie Zhou, and Jiwen Lu. Label2label: A language modeling framework for multi-attribute learning. In *European Conference on Computer Vision*, pages 562–579. Springer, 2022.

[109] Jian Jia, Naiyu Gao, Fei He, Xiaotang Chen, and Kaiqi Huang. Learning disentangled attribute representations for robust pedestrian attribute recognition. 2022.

[110] MMPose Contributors. Openmmlab pose estimation toolbox and benchmark. <https://github.com/open-mmlab/mmpose>, 2020.

[111] Haodong Duan, Yue Zhao, Kai Chen, Dahua Lin, and Bo Dai. Revisiting skeleton-based action recognition. In *Proceedings of the IEEE/CVF Conference on Computer Vision and Pattern Recognition*, pages 2969–2978, 2022.

[112] Jun Liu, Amir Shahroudy, Mauricio Perez, Gang Wang, Ling-Yu Duan, and Alex C Kot. Ntu rgb+ d 120: A large-scale benchmark for 3d human activity understanding. *IEEE transactions on pattern analysis and machine intelligence*, 42(10):2684–2701, 2019.

[113] Sijie Yan, Yuanjun Xiong, and Dahua Lin. Spatial temporal graph convolutional networks for skeleton-based action recognition. In *Proceedings of the AAAI conference on artificial intelligence*, volume 32, 2018.

[114] Maosen Li, Siheng Chen, Xu Chen, Ya Zhang, Yanfeng Wang, and Qi Tian. Actional-structural graph convolutional networks for skeleton-based action recognition. In *Proceedings of the IEEE/CVF conference on computer vision and pattern recognition*, pages 3595–3603, 2019.

[115] Lei Shi, Yifan Zhang, Jian Cheng, and Hanqing Lu. Two-stream adaptive graph convolutional networks for skeleton-based action recognition. In *Proceedings of the IEEE/CVF conference on computer vision and pattern recognition*, pages 12026–12035, 2019.

[116] Ke Cheng, Yifan Zhang, Xiangyu He, Weihan Chen, Jian Cheng, and Hanqing Lu. Skeleton-based action recognition with shift graph convolutional network. In *Proceedings of the IEEE/CVF conference on computer vision and pattern recognition*, pages 183–192, 2020.

[117] Linguo Li, Minsi Wang, Bingbing Ni, Hang Wang, Jiancheng Yang, and Wenjun Zhang. 3d human action representation learning via cross-view consistency pursuit. In *Proceedings of the IEEE/CVF conference on computer vision and pattern recognition*, pages 4741–4750, 2021.

[118] Yukun Su, Guosheng Lin, and Qingyao Wu. Self-supervised 3d skeleton action representation learning with motion consistency and

continuity. In *Proceedings of the IEEE/CVF international conference on computer vision*, pages 13328–13338, 2021.

[119] Siyuan Yang, Jun Liu, Shijian Lu, Meng Hwa Er, and Alex C Kot. Skeleton cloud colorization for unsupervised 3d action representation learning. In *Proceedings of the IEEE/CVF International Conference on Computer Vision*, pages 13423–13433, 2021.

[120] Di Yang, Yaohui Wang, Antitza Dantcheva, Lorenzo Garattoni, Giampiero Francesca, and François Brémond. Unik: A unified framework for real-world skeleton-based action recognition. *arXiv preprint arXiv:2107.08580*, 2021.

[121] Yuxin Chen, Ziqi Zhang, Chunfeng Yuan, Bing Li, Ying Deng, and Weiming Hu. Channel-wise topology refinement graph convolution for skeleton-based action recognition. In *Proceedings of the IEEE/CVF international conference on computer vision*, pages 13359–13368, 2021.

[122] Ziyu Liu, Hongwen Zhang, Zhenghao Chen, Zhiyong Wang, and Wanli Ouyang. Disentangling and unifying graph convolutions for skeleton-based action recognition. In *Proceedings of the IEEE/CVF conference on computer vision and pattern recognition*, pages 143–152, 2020.

[123] Shuai Li, Wanqing Li, Chris Cook, Ce Zhu, and Yanbo Gao. Independently recurrent neural network (indrnn): Building a longer and deeper rnn. In *Proceedings of the IEEE conference on computer vision and pattern recognition*, pages 5457–5466, 2018.

[124] QiuHong Ke, Mohammed Bennamoun, Senjian An, Ferdous Sohel, and Farid Boussaid. Learning clip representations for skeleton-based 3d action recognition. *IEEE Transactions on Image Processing*, 27(6):2842–2855, 2018.

[125] Chao Li, Qiaoyong Zhong, Di Xie, and Shiliang Pu. Co-occurrence feature learning from skeleton data for action recognition and detection with hierarchical aggregation. *arXiv preprint arXiv:1804.06055*, 2018.

[126] Chiara Plizzari, Marco Cannici, and Matteo Matteucci. Skeleton-based action recognition via spatial and temporal transformer networks. *Computer Vision and Image Understanding*, 208:103219, 2021.

[127] Lei Shi, Yifan Zhang, Jian Cheng, and Hanqing Lu. Decoupled spatial-temporal attention network for skeleton-based action-gesture recognition. In *Proceedings of the Asian Conference on Computer Vision*, 2020.

[128] Helei Qiu, Biao Hou, Bo Ren, and Xiaohua Zhang. Spatio-temporal tuples transformer for skeleton-based action recognition. *arXiv preprint arXiv:2201.02849*, 2022.

[129] Junnan Li, Dongxu Li, Caiming Xiong, and Steven Hoi. Blip: Bootstrapping language-image pre-training for unified vision-language understanding and generation. In *International Conference on Machine Learning*, pages 12888–12900. PMLR, 2022.

[130] Zhihao Li, Jianzhuang Liu, Zhensong Zhang, Songcen Xu, and Youliang Yan. Cliff: Carrying location information in full frames into human pose and shape estimation. In *European Conference on Computer Vision*, pages 590–606. Springer, 2022.

[131] Angjoo Kanazawa, Michael J Black, David W Jacobs, and Jitendra Malik. End-to-end recovery of human shape and pose. In *Proceedings of the IEEE conference on computer vision and pattern recognition*, pages 7122–7131, 2018.

[132] Nikos Kolotouros, Georgios Pavlakos, and Kostas Daniilidis. Convolutional mesh regression for single-image human shape reconstruction. In *Proceedings of the IEEE/CVF Conference on Computer Vision and Pattern Recognition*, pages 4501–4510, 2019.

[133] Nikos Kolotouros, Georgios Pavlakos, Michael J Black, and Kostas Daniilidis. Learning to reconstruct 3d human pose and shape via model-fitting in the loop. In *Proceedings of the IEEE/CVF international conference on computer vision*, pages 2252–2261, 2019.

[134] Gyeongsik Moon and Kyoung Mu Lee. I2l-meshnet: Image-to-lixel prediction network for accurate 3d human pose and mesh estimation from a single rgb image. In *Computer Vision–ECCV 2020: 16th European Conference, Glasgow, UK, August 23–28, 2020, Proceedings, Part VII 16*, pages 752–768. Springer, 2020.

[135] Hongwen Zhang, Yating Tian, Xinchu Zhou, Wanli Ouyang, Yebin Liu, Limin Wang, and Zhenan Sun. Pymaf: 3d human pose and shape regression with pyramidal mesh alignment feedback loop. In *Proceedings of the IEEE/CVF International Conference on Computer Vision*, pages 11446–11456, 2021.

[136] Yu Sun, Qian Bao, Wu Liu, Yili Fu, Michael J Black, and Tao Mei. Monocular, one-stage, regression of multiple 3d people. In *Proceedings of the IEEE/CVF international conference on computer vision*, pages 11179–11188, 2021.

[137] Muhammed Kocabas, Chun-Hao P Huang, Otmar Hilliges, and Michael J Black. Pare: Part attention regressor for 3d human body estimation. In *Proceedings of the IEEE/CVF International Conference on Computer Vision*, pages 11127–11137, 2021.

[138] Kevin Lin, Lijuan Wang, and Zicheng Liu. End-to-end human pose and mesh reconstruction with transformers. In *Proceedings of the IEEE/CVF conference on computer vision and pattern recognition*, pages 1954–1963, 2021.

[139] Kevin Lin, Lijuan Wang, and Zicheng Liu. Mesh graphomer. In *Proceedings of the IEEE/CVF international conference on computer vision*, pages 12939–12948, 2021.

[140] Nikos Kolotouros, Georgios Pavlakos, Dinesh Jayaraman, and Kostas Daniilidis. Probabilistic modeling for human mesh recovery. In *Proceedings of the IEEE/CVF international conference on computer vision*, pages 11605–11614, 2021.

[141] Rawal Khirodkar, Shashank Tripathi, and Kris Kitani. Occluded human mesh recovery. In *Proceedings of the IEEE/CVF conference on computer vision and pattern recognition*, pages 1715–1725, 2022.

[142] Hongsuk Choi, Gyeongsik Moon, JoonKyu Park, and Kyoung Mu Lee. Learning to estimate robust 3d human mesh from in-the-wild crowded scenes. In *Proceedings of the IEEE/CVF Conference on Computer Vision and Pattern Recognition*, pages 1475–1484, 2022.

[143] Junhyeong Cho, Kim Youwang, and Tae-Hyun Oh. Cross-attention of disentangled modalities for 3d human mesh recovery with transformers. In *European Conference on Computer Vision*, pages 342–359. Springer, 2022.

[144] Chun-Han Yao, Jimei Yang, Duygu Ceylan, Yi Zhou, Yang Zhou, and Ming-Hsuan Yang. Learning visibility for robust dense human body estimation. In *European Conference on Computer Vision*, pages 412–428. Springer, 2022.

## APPENDIX A FULL ABLATION RESULTS

As shown in Table XVI, we present the full experimental results of the ablation studies. Specifically, we explore the affects of (1) different weight sharing strategies, (2) attention mask designs in decoder, (3) task collaboration and interference, and (4) different initialization weights. One can see that the same conclusion can be observed that as more model components are shared, Hulk can achieve higher performance. Besides, omitting any task generally leads to reduced performance. Furthermore, employing different attention interaction methods for different tasks can optimize the model’s performance, compared with using pure full attention or diagonal attention. Last, using the pre-trained weights from other human-centric models (i.e., HAP [30] and PATH [29]) can further boost our hulk’s performance. This result not only validates the robustness of Hulk but also highlight its potential for further enhancement.

Moreover, in Table XVII, to assess the impact of the diverse and sufficient human-centric data, we train Hulk using a 60000-iteration schedule on the ablation datasets comprising 1.7M training samples, and full datasets comprising 30M training samples, respectively. Results indicate that incorporating more human-centric data and increasing the training iterations brings considerable performance improvement across all tasks.

## APPENDIX B ADDITIONAL ARCHITECTURE DETAILS

### A. Modality indicator

Modality indicators  $\mathcal{I}_{m'}$  are learnable tokens that are appended with encoded tokens  $\mathbf{p}$  to generate the output tokens  $\mathbf{q}$  through the modality-shared decoder. In the decoder, modality indicators  $\mathcal{I}_{m'}$  have a default shape of  $\mathcal{R}^{1 \times d_{out}}$ , where  $d_{out}$  is the dimension of output tokens. For a certain task that requires  $N'$  output tokens, we repeat the modality indicator  $N'$  times, resulting in a shape of  $\mathcal{R}^{N' \times d_{out}}$ .

1) *Weight sharing.*: As an indicator, modality indicators  $\mathcal{I}_{m'}$  are shared within the same modality but across different tasks, *e.g.*, the dense labeling modality indicator  $\mathcal{I}_D$  is utilized for both human parsing task and 2D pose estimation task. This design together with the modality-shared encoder and decoder helps Hulk learn human-centric knowledge, remedying task bias from a certain task.

2) *Shape of modality indicators.*: While the aligning text features  $\mathbf{v} \in \mathcal{R}^{C \times d_{out}}$  always have a length of  $C$  denoting the number of semantics/classes,  $N'$  varies among different human-centric tasks. For **action and attribute recognition tasks**,  $N' = C$  where  $C$  is the number of action or attribute classes. After aligning with BERT semantic features  $\mathbf{v}$ , the similarity in the  $i$ -th index represents the existence probability of the  $i$ -th action/attribute. For the **image caption task**,  $N' = 40$  means the length of caption tokens. For dense label output tasks, *i.e.*, **human parsing and 2D pose estimation tasks**,  $N'$  equals the number of input image tokens  $N$ , generating predicted semantic maps with the same resolution. For sparse label output tasks, *i.e.*, **pedestrian detection, 3D**

**pose estimation, and mesh recovery task**,  $N'$  equals the number of predicted boxes/joints/vertices.

### B. Positional Embeddings

1) *Positional embeddings in the encoder*: Different from UniHCP [2], we do not use a learnable positional embedding, instead, we use the bilinear interpolation of fixed MAE [96] positional embeddings in the encoder.

2) *Positional embeddings in the decoder*: As the inputs for the decoder contain two parts, *i.e.*, encoded tokens  $\mathbf{p}$  and modality indicator  $\mathcal{I}_{m'}$ , therefore, positional embeddings in the decoder have two parts.

For the encoded tokens part, positional embeddings are set as the bilinear interpolation of fixed MAE positional embeddings.

For the modality indicator part, we prepare three types of positional embeddings for better experimental results across diverse human-centric tasks:

- **Anchor points**. For the pedestrian detection task, we follow anchor DETR [?] to integrate the location information into modality indicators for achieving better performance. To ensure compatibility with the MAE positional embeddings, which have a shape of  $14 \times 14$ , used in the encoded tokens part, we generate  $17 \times 17$  positional embeddings as fixed anchor points. This approach enables Hulk to focus on regressing the distances between these anchor points and the actual ground truth boxes. By doing so, the detection task is simplified, effectively reducing the complexity and difficulty of convergence.

- **3D positional embeddings**. For 3D pose estimation and mesh recovery tasks, Hulk needs to predict 3D digit locations using 3D positional embeddings. Following the practice in [?], we separate the 3D positional embeddings into a fixed  $2D$  positional embedding and a fixed  $1D$  positional embedding with  $PE_{3D} = PE_{2D} + PE_{1D}$ , introducing strong 3D location information into 3D regression tasks. The  $2D$  positional embedding and  $1D$  positional embedding can be generated by interpolating from fixed MAE positional embeddings.

- **Simple interpolation**. For tasks encompassing 2D vision, vision-language, and skeleton-based applications, we employ a straightforward approach to generate the positional embeddings in the modality indicator part. These embeddings are inherently two-dimensional or one-dimensional and are derived through a process of simple interpolation from the fixed MAE positional embeddings.

### C. Objective function details

In this section, we present the objective functions in Sec. IV.D in the main text. Given the prediction  $\hat{\mathbf{y}}'_m$  where  $m' \in \{I, T, S, D\}$  is the output modality, we compute the losses according to different human-centric tasks. As modality-specific de-tokenizers transform output tokens to the semantic part and the digital location part, we adopt two types of losses, *i.e.*, semantic contrastive loss and digit regression loss.

For **semantic constrasitive loss**, we first compute the conv-transformed output tokens  $\hat{\mathbf{f}} \in \mathbb{R}^{N' \times d_{out}}$  with  $\hat{\mathbf{f}} = \text{Conv}(\mathbf{q})$ ,

TABLE XVI

COMPLETE EXPERIMENTAL RESULTS OF DIFFERENT ABLATION STUDIES. THE AVERAGE PERFORMANCES IN THE ABLATION OF TASK COLLABORATION AND INTERFERENCE ARE NOT COMPUTED AND REPLACED BY N/A.

Methods	Parsing			2D Pose		Detection		Attribute		Caption		Skeleton		3D Pose & Mesh						Avg.
	H3.6	LIP	CIHP	COCO	AIC	Crowd	PA	rapv2	CUHK	ntu60	Human3.6M						3DPW			
	mIoU	mIoU	mIoU	AP	AP	AP	mA	mA	B@4	Acc	100-MPJPE	100-PA-MPJPE	100-MPVPE	100-MPJPE	100-PA-MPJPE	100-PA-MPJPE	100-PA-MPJPE	100-PA-MPJPE		
(a) baseline (Hulk)	62.4	56.8	59.7	70.8	25.5	81.8	79.4	77.9	28.0	93.2	45.9	60.5	-0.3	13.2	49.0	53.6				
<i>Weight sharing</i>																				
(b) only enc./dec. shared	63.4	56.8	59.6	71.1	25.8	80.6	80.8	78.8	26.7	93.8	45.2	60.3	-3.0	10.7	47.0	53.2				
(c) only enc. shared	51.6	56.3	60.5	71.3	25.7	75.9	82.2	81.3	28.7	1.7	35.9	56.5	-11.2	2.9	41.3	44.0				
<i>Attention Mask Designs in the Decoder</i>																				
full-att	62.6	57.2	59.9	70.9	25.4	79.9	79.2	77.6	28.6	91.8	44.3	60.1	-1.0	13.4	48.1	53.2				
diag-att	62.7	56.6	59.9	70.6	25.6	80.3	79.3	78.0	28.4	93.1	46.3	57.6	-4.1	10.0	46.3	52.3				
<i>Task Collaboration and Interference</i>																				
w/o attribute	62.4	56.9	59.9	70.7	25.6	79.9	-	-	28.2	93.1	44.4	60.0	-2.1	12.2	47.9	N/A				
w/o caption	62.7	57.3	59.9	70.7	25.6	80.2	79.3	77.8	-	92.9	46.5	61.3	-2.2	11.2	47.5	N/A				
w/o skeleton	62.3	57.4	60.1	70.7	25.7	80.9	79.1	77.4	28.2	-	45.7	59.6	-4.8	10.0	46.7	N/A				
w/o mesh&3d pose	62.6	57.4	60.3	70.8	25.5	81.0	79.8	78.0	27.9	93.1	-	-	-	-	-	N/A				
w/o detection	63.2	57.6	60.9	71.4	26.4	-	79.9	77.6	27.8	93.1	46.0	59.8	-4.8	10.5	47.6	N/A				
w/o 2d pose	56.6	52.3	53.0	-	-	65.0	75.3	75.1	26.6	93.5	24.5	48.4	-18.9	-3.5	37.2	N/A				
w/o parsing	-	-	-	70.2	25.2	78.5	79.4	77.3	25.8	93.2	42.5	57.5	-2.9	10.8	46.7	N/A				
<i>Different initialization weights</i>																				
MAE (baseline)	62.4	56.8	59.7	70.8	25.5	81.8	79.4	77.9	28.0	93.2	45.9	60.5	-0.3	13.2	49.0	53.6				
HAP	65.8	63.3	68.8	76.5	33.4	85.4	85.5	81.8	29.6	91.5	55.2	66.6	9.6	22.9	55.6	59.4				
PATH	66.3	63.6	69.2	76.8	34.5	88.6	83.3	80.2	29.9	92.8	54.6	66.7	8.3	21.3	54.5	59.4				

TABLE XVII

COMPLETE EXPERIMENTAL RESULTS OF OUR HULK PERFORMANCE ON DIVERSE HUMAN-CENTRIC TASKS WHEN SCALING UP DATA SIZE. EXPERIMENTS ARE BOTH TRAINED WITH A **FULL 60,000-ITERATION** SCHEDULE, SHOWING THAT LEARN FROM ADDITIONAL DATA AND ACHIEVE BETTER PERFORMANCE ON AVERAGE. .

Methods	Parsing			2D Pose		Detection		Attribute		Caption		Skeleton		3D Pose & Mesh						Avg
	H3.6	LIP	CIHP	COCO	AIC	Crowd	PA	rapv2	CUHK	ntu60	Human3.6M						3DPW			
	mIoU	mIoU	mIoU	AP	AP	AP	mA	mA	B@4	Acc	100-MPJPE	100-PA-MPJPE	100-MPVPE	100-MPJPE	100-PA-MPJPE	100-PA-MPJPE	100-PA-MPJPE	100-PA-MPJPE		
30M	68.1	64.0	70.6	77.0	34.5	90.7	82.9	80.9	31.1	93.8	56.4	68.1	20.2	33.0	60.1	62.1				
1.7M	66.9	63.5	68.4	76.0	32.2	89.1	82.1	80.8	29.0	93.7	36.0	60.3	-5.8	8.5	44.9	55.0				

where  $N'$  is the number of output tokens,  $d_{out}$  is the output dimension, and  $\mathbf{q} \in \mathbb{R}^{N' \times d_{out}}$  are output tokens. Given  $\mathbf{v} = (\mathbf{v}_1, \mathbf{v}_2, \dots, \mathbf{v}_C)$  containing the BERT features of  $C$  ground truth classes, the semantic contrastive loss is defined as

$$\mathcal{L}^s = \frac{\mathbf{v}_k^\top \hat{\mathbf{f}}}{\mathbf{v}_1^\top \hat{\mathbf{f}} + \mathbf{v}_2^\top \hat{\mathbf{f}} + \dots + \mathbf{v}_C^\top \hat{\mathbf{f}}}, \quad (18)$$

where  $k$  is the index of the selected semantic token.

For **digit regression loss**, we compute the distance between predicted coordinate values  $\hat{\mathbf{y}}^d$  and corresponding ground truth coordinate values  $\mathbf{y}^d$  with

$$\mathcal{L}^d = Dis(\hat{\mathbf{y}}^d, \mathbf{y}^d), \quad (19)$$

where  $Dis(\mathbf{a}, \mathbf{b})$  measures the distance between  $\mathbf{a}$  and  $\mathbf{b}$ , which is different in different tasks, *i.e.*, L1 loss and GIoU loss in the pedestrian detection.

**Human Parsing.** Human parsing aims to segment human parts. As human parts can be represented by their BERT features, we align the output tokens with BERT features of semantic classes using per-pixel contrastive loss. Following the practice in UniHCP [2], we also supervise the global probability of a certain semantic class to enhance the performance. Given the conv-transformed output tokens  $\hat{\mathbf{f}}$ , we simply average pool them to represent the predicted probability of occurrence of certain semantic class  $\hat{\mathbf{f}}_{avg}$ . Given extracted BERT features  $\mathbf{v}$  of  $C$  parsing classes, , the total objective function for human parsing is as follows:

$$\mathcal{L}_{par} = \mathcal{L}^s(\hat{\mathbf{f}}, \mathbf{v}_{pix}) + \mathcal{L}^s(\hat{\mathbf{f}}_{avg}, \mathbf{v}) + \mathcal{L}_{dice}(\hat{\mathbf{y}}, \mathbf{y}), \quad (20)$$

where  $\mathbf{v}_{pix} \in \mathbb{R}^{N \times C \times d_{out}}$  denotes the per-pixel BERT features,  $\mathcal{L}_{dice}$  is adopted as an auxiliary loss to enhance the human parsing performance. In the dice loss,  $\mathbf{y} \in \mathbb{R}^{N \times C}$  denotes the ground truth heatmaps with  $C$  parsing classes and  $\hat{\mathbf{y}}_D \in \mathbb{R}^{N \times C}$  is the predicted heatmaps computed by  $\hat{\mathbf{y}} = \{\hat{\mathbf{y}}_j = \text{argmax}_{k \in [1, C]} \mathbf{v}^\top \text{Upsample}(\hat{\mathbf{f}}_j)\}, j \in [1, N']$ .

**2D Pose Estimation.** We follow the common top-down setting for 2D pose estimation. As we leverage the heatmap-based methods for 2D pose estimation for better experimental results, the objective function is similar to that in human parsing. Mathematically, given extracted BERT features  $\mathbf{v}$  of  $C$  joint names, we have

$$\mathcal{L}_{pose} = \mathcal{L}^s(\hat{\mathbf{f}}, \mathbf{v}_{pix}) + \mathcal{L}^s(\hat{\mathbf{f}}_{avg}, \mathbf{v}), \quad (21)$$

where  $\mathbf{v}_{pix} \in \mathbb{R}^{N \times C \times d_{out}}$  denotes the per-pixel BERT features.

**Pedestrian Attribute Recognition.** Pedestrian Attribute Recognition predicts whether an attribute exists in the input image. Therefore, we only supervise the output tokens  $\hat{\mathbf{f}} \in \mathbb{R}^{C \times d_{out}}$  by aligning them to  $C$  different attribute semantics. High similarity means the existence of a certain attribute. Given extracted attribute BERT features  $\mathbf{v} \in \mathbb{R}^{C \times d_{out}}$ , the objective function can be computed by:

$$\mathcal{L}_{attr} = \mathcal{L}^s(\hat{\mathbf{f}}, \mathbf{v}). \quad (22)$$

**Pedestrian Image Caption.** We predict the image caption in an auto-regressive manner. For each predicted token, we

adopt the semantic contrastive loss  $\mathcal{L}^s$  to supervise. The total objective function is similar to that in attribute recognition,

$$\mathcal{L}_{cap} = \mathcal{L}^s(\hat{\mathbf{f}}, \mathbf{v}), \quad (23)$$

where  $\hat{\mathbf{f}} \in \mathbb{R}^{N' \times d_{out}}$  are the features representing predicted caption tokens,  $N'$  is 40 by default.  $\mathbf{v} \in \mathbb{R}^{C \times d_{out}}$  denotes the features of BERT vocabulary, where  $C = 30522$  denotes the length of BERT vocabulary.

**Pedestrian Detection.** Different from widely adopted designs in transformer-based pedestrian detectors that rely on object queries, we directly decode  $N'$  modality indicators as the sparse prediction results. Given predicted digital location  $\hat{\mathbf{y}}^d$ , predicted semantic features  $\hat{\mathbf{f}}$ , ground truth location  $\mathbf{y}^d$  and ground truth semantic features  $\mathbf{v}$  representing the word “pedestrian”, we utilize optimal bipartite matching to determine the matched pairs. The objective function can be computed by the combination of semantic contrastive loss and digit regression loss:

$$\mathcal{L}_{det} = \mathcal{L}_{L1}(\hat{\mathbf{y}}^d, \mathbf{y}^d) + \mathcal{L}_{iou}(\hat{\mathbf{y}}^d, \mathbf{y}^d) + \mathcal{L}^s(\hat{\mathbf{f}}, \mathbf{v}), \quad (24)$$

where  $\mathcal{L}_{L1}$ ,  $\mathcal{L}_{iou}$  are L1 loss and GIoU loss, respectively.

**3D Pose Estimation & Mesh Recovery.** Following common practice [130], [138], [143], we train Hulk to learn 3D pose estimation task and mesh recovery task jointly. Similar to the pedestrian detection task, the 3D pose estimation task also has a combined objective function of semantic contrastive loss and digital regression loss while the mesh recovery task only has the digit regression loss due to undefined semantics of numerous vertices. Given predicted digital location  $\hat{\mathbf{y}}^d$ , predicted semantic features  $\hat{\mathbf{f}}$  representing  $C$  different joint semantics, we compute the objective function for 3D pose estimation and mesh recovery as

$$\begin{aligned} \mathcal{L}_{3dpos} + \mathcal{L}_{mesh} = & \mathcal{L}_{2d}(\hat{\mathbf{y}}^d, \mathbf{y}) + \mathcal{L}_{3d}(\hat{\mathbf{y}}^d, \mathbf{y}) \\ & + \mathcal{L}_{vertex}(\hat{\mathbf{y}}^d, \mathbf{y}) + \mathcal{L}_{normal}(\hat{\mathbf{y}}^d, \mathbf{y}) \\ & + \mathcal{L}_{edge}(\hat{\mathbf{y}}^d, \mathbf{y}) + \mathcal{L}^s(\hat{\mathbf{f}}, \mathbf{v}), \end{aligned} \quad (25)$$

where  $\mathbf{y}$  is the ground truth location,  $\mathbf{v}$  denotes BERT features of joint names.  $\mathcal{L}_{2d}$ ,  $\mathcal{L}_{3d}$ ,  $\mathcal{L}_{vertex}$ ,  $\mathcal{L}_{normal}$ , and  $\mathcal{L}_{edge}$  are all L1 loss.

**Skeleton-based action Recognition.** Skeleton-based action recognition predicts the action based on input skeleton sequence. Therefore, given action semantic features  $\mathbf{v} \in \mathbb{R}^{C \times d_{out}}$  where  $C$  is the number of actions, and the predicted semantic tokens  $\hat{\mathbf{f}} \in \mathbb{R}^{C \times d_{out}}$ , the objective function can be computed by:

$$\mathcal{L}_{ske} = \mathcal{L}^s(\hat{\mathbf{f}}, \mathbf{v}). \quad (26)$$

## APPENDIX C DETAILS OF TRAINING DATASETS

### A. Full setting

As shown in Table XVIII, we utilize 42 publically available datasets to form the training set for training our Hulk model, containing 30,187,836 training samples and covering eight different human-centric tasks, including human parsing, 2D pose estimation, attribute recognition, pedestrian detection, skeleton-based action recognition, image caption, 3D pose estimation, and mesh recovery.

TABLE XVIII  
STATISTICS OF TRAINING DATASETS IN THE FULL SETTING.

Task type	Dataset	Number of samples
Human parsing (7 datasets)	Human3.6M [64]	62,668
	LIP [65]	30,462
	CIHP [66]	28,280
	ModaNet [?]	52,245
	VIP [?]	18,469
	Deep fashion [?]	191,961
	Paper Doll [?]	1,035,825
2D pose estimation (8 datasets)	COCO [67]	149,813
	AIC [68]	378,352
	Human3.6M (pose) [64]	312,187
	Posetrack [69]	97,174
	3DPW [83]	68,663
	JRDB-Pose [?]	139,385
	MPI-INF-3DHP [?]	1,031,701
	AIST++ [?]	1,015,257
Attribute recognition (6 datasets)	RAPv2 [70]	67,943
	PA_100k [71]	90,000
	Parse27k [72]	27,482
	Market [?]	12,926
	HARDHC [?]	28,336
	LU-Person [6]	10,684,342
Pedestrian detection (6 datasets)	CrowdHuman [73]	15,000
	EuroCity [74]	21,785
	CityPersons [?]	2,778
	WiderPerson [75]	9,000
	WiderPedestrian [?]	58,009
	COCO-person [67]	64,115
Skeleton-based action (6 datasets)	NTU60 [76]	40,091
	NTU120 [112]	63,026
	GYM [77]	2,778
	Diving48 [78]	15,027
	UCF101 [?]	13,320
	Kinetics-400 [?]	239,737
Image caption (2 datasets)	CUHK-PEDS [79]	68,126
	SYNTH-PEDES [80]	12,138,157
3D pose & Mesh (7 datasets)	Human3.6M [64]	312,188
	3DPW [83]	22,735
	COCO [67]	40,055
	MUCO [81]	101,883
	UP-3D [?]	7,126
	MPII [92]	14,810
	GTA [82]	1,396,913
Total	42	30,187,836 $\approx$ 30M

### B. Ablation setting

In ablation studies, to demonstrate the effectiveness of Hulk and further explore the potential of a human-centric foundation model, we conduct several ablations on a smaller training set. In Table XIX, the ablation set consists of 21 datasets with about 1.7M samples, covering all eight tasks.

## APPENDIX D DETAILS OF DATASET-WISE CONFIGURATIONS

### A. Training

We provide detailed dataset-wise training configurations in Table XX, including total batch size, batch size per GPU, the number of GPUs, and task weights. In order to better unify different tasks and different datasets, the different datasets of certain tasks (i.e., attribute recognition, pedestrian detection, skeleton-based action, image caption, 3D pose and mesh

TABLE XIX  
STATISTICS OF TRAINING DATASETS IN THE ABLATION SETTING.

Task type	Dataset	Number of samples
Human parsing (3 datasets)	Human3.6M [64]	62,668
	LIP [65]	30,462
	CIHP [66]	28,280
2D pose estimation (2 datasets)	COCO [67]	149,813
	AIC [68]	378,352
Attribute recognition (5 datasets)	RAPv2 [70]	67,943
	PA_100k [71]	90,000
	Parse27k [72]	27,482
	Market [?]	12,926
	HARDHC [?]	28,336
Pedestrian detection	CrowdHuman [73]	15,000
Skeleton action (2 datasets)	NTU60 [76]	40,091
	NTU120 [112]	63,026
Image caption (2 datasets)	CUHK-PEDS [79]	68,126
	SYNTH-PEDES [80]	132,000
3D pose & Mesh (6 datasets)	Human3.6M [64]	312,188
	3DPW [83]	22,735
	COCO [67]	40,055
	MUCO [81]	101,883
	UP-3D [?]	7,126
	MPII [92]	14,810
Total	21	1,693,302 $\approx$ <b>1.7M</b>

recovery) are stacked together as a integrated dataset for training, and the datasets of some other tasks (i.e., human parsing and 2D pose estimation) are separately trained on different GPUs with diverse task weights.

### B. Fine-tuning

For fine-tuning porcess, we carefully tune the learning rate, total batch size, the number of iterations, and drop path rate, and report the best performances. In details, the ViT-base backbone (i.e., in Table XXI) and ViT-large backbone (i.e., in Table XXII) are tuned, respectively.

TABLE XX  
HULK JOINT TRAINING SETUP.

Task Type	Dataset	Batch Size	Batch Size per GPU	GPUs	Task Weight
Human parsing	LIP	108	27	4	1.8
	CIHP	104	26	4	3.6
	Human3.6M	217	31	7	2.25
	ModaNet	27	27	1	0.021
	VIP	27	27	1	0.021
	Deepfashion	54	27	2	0.042
	PaperDoll	27	27	1	0.021
2D pose estimation	COCO	528	176	3	28000
	AIC	1323	189	7	56000
	Human3.6M	264	132	2	3192
	Posetrack	340	170	2	12335
	JRDB	340	170	2	8223
	MPI-INF-3DHP	340	170	2	8223
	3DPW	170	170	1	2055
	AIST++	170	170	1	2055
	RAPv2				
Attribute recognition	PA				
	Parse27k	147	147	1	5
	Market				
	HARDHC				
	LUPerson	300	300	1	5
Pedestrian detection	CrowdHuman	32	4	8	15
	EuroCity				
	CityPersons				
	WiderPerson	80	4	20	42.4
	WiderPedestrian				
Skeleton action	COCO				
	Ntu60				
	Ntu120	240	120	2	4.4
	gym				
Image caption	Diving48				
	UCF101	90	90	1	1
	K400				
3D pose & Mesh	SYNTH-PEDES	300	100	3	90
	CUHK-PEDES				
3D pose & Mesh	3DPW				
	Human3.6M				
	COCO				
	mMUCOuco	495	165	3	0.5
	UP-3D				
	MPII				
	GTA				

TABLE XXI  
DETAILED FINETUNING CONFIGS WITH VIT-BASE BACKBONE FOR HUMAN-CENTRIC TASKS.

Task Type	Dataset	Learning Rate	Batch Size	Iterations	Drop Path Rate
2D pose estimation	COCO	3.00E-05	1024	20k	0.3
	AIC	3.00E-04	1024	15k	0.2
3D pose & Mesh	3DPW	3.00E-05	512	10k	0.2
	Human3.6M	3.00E-05	512	10k	0.2
Pedestrian detection	CrowdHuman	1.00E-04	32	80k	0.2
Human parsing	LIP	1.00E-04	1024	20k	0.3
	CIHP	1.00E-04	1024	20k	0.3
	Human3.6M	5.00E-04	1024	20k	0.3
Attribute recognition	RAPv2	6.00E-04	128	8k	0.2
	PA	3.00E-04	128	5k	0.2
Skeleton action	NTU60	1.00E-04	48	10k	0.2
Image caption	CUHK-PEDES	1.00E-06	256	3k	0.2

TABLE XXII  
DETAILED FINETUNING CONFIGS WITH **ViT-LARGE BACKBONE** FOR HUMAN-CENTRIC TASKS.

Task Type	Dataset	Learning Rate	Batch Size	Iterations	Drop Path Rate
2D pose estimation	COCO	3.00E-05	1024	10k	0.6
	AIC	3.00E-04	1024	15k	0.3
3D pose & Mesh	3DPW	3.00E-05	512	10k	0.2
	Human3.6M	3.00E-05	512	10k	0.2
Pedestrian detection	CrowdHuman	1.00E-04	32	10k	0.5
Human parsing	LIP	5.00E-05	512	10k	0.5
	CIHP	5.00E-05	512	10k	0.5
	Human3.6M	1.00E-05	512	10k	0.5
Attribute recognition	RAPv2	1.00E-03	128	6k	0.5
	PA	7.00E-04	128	3k	0.5
Skeleton action	NTU60	1.00E-05	48	10k	0.5
Image caption	CUHK-PEDES	1.00E-06	256	3k	0.5